Recovery of Oligomers and Cooperativity When Monomers of the M_2 Muscarinic Cholinergic Receptor Are Reconstituted into Phospholipid Vesicles†

Amy W.-S. Ma, Dar'ya S. Redka, Luca F. Pisterzi, Stéphane Angers, and James W. Wells*

Department of Pharmaceutical Sciences, Leslie Dan Faculty of Pharmacy, University of Toronto, Toronto, Ontario, Canada M5S 3M2

Received December 19, 2006; Revised Manuscript Received March 30, 2007

ABSTRACT: FLAG- and HA-tagged M_2 muscarinic receptors from coinfected *Sf*9 cells have been purified in digitonin−cholate and reconstituted into phospholipid vesicles. The purified receptor was predominantly monomeric: it showed no detectable coimmunoprecipitation; it migrated as a monomer during electrophoresis before or after cross-linking with *bis*(sulfosuccinimidyl)suberate; and it bound agonists and antagonists in a manner indicative of identical and mutually independent sites. Receptor cross-linked after reconstitution or after reconstitution and subsequent solubilization in digitonin−cholate migrated almost exclusively as a tetramer. The binding properties of the reconstituted receptor mimicked those reported previously for cardiac muscarinic receptors. The apparent capacity for *N*-[^{3}H]methylscopolamine (NMS) was only 60% of that for [^{3}H]quinuclidinylbenzilate (QNB), yet binding at saturating concentrations of [^{3}H]QNB was inhibited fully and in a noncompetitive manner at comparatively low concentrations of unlabeled NMS. Reconstitution of the receptor with a saturating quantity of functional G proteins led to the appearance of three classes of sites for the agonist oxotremorine-M in assays with [^{3}H]QNB; GMP-PNP caused an apparent interconversion from highest to lowest affinity and the concomitant emergence of a fourth class of intermediate affinity. All of the data can be described quantitatively in terms of cooperativity among four interacting sites, presumably within a tetramer; the effect of GMP-PNP can be accommodated as a shift in the distribution of tetramers between two states that differ in their cooperative properties. Monomers of the M_2 receptor therefore can be assembled into tetramers with binding properties that closely resemble those of the muscarinic receptor in myocardial preparations.

Signaling via G protein-coupled receptors is controlled by an allosteric interaction between agonists and guanyl nucleotides (*1*, *2*). The underlying mechanism remains obscure, but two observations may offer some insight. First, many G protein-coupled receptors have been shown to occur as oligomers, both on living cells and following extraction from the membrane (reviewed in *3*−*5*); second, at least some have been found to exhibit cooperative effects in the binding of agonists and antagonists. The latter observation implies the former and has implications for our understanding of the mechanistically ambiguous, GTP-sensitive dispersion of affinities seen almost universally in the binding of agonists (*6*). Those effects are linked to efficacy (e.g., refs *7*−*9*), and they can be described in terms of cooperativity between two or more interacting sites (*6*, *10*).

For many years, the common view of G protein-mediated signaling was based on the notion of a ligand-regulated, transient complex between one holo-G protein (G) and one receptor (R) (*1*, *11*). As articulated in the ternary complex model (*12*), the receptor interconverts spontaneously between G protein-coupled (RG) and uncoupled states. Agonists bind with higher affinity to RG than to R, thereby favoring the coupled state; in contrast, guanyl nucleotides bind with higher affinity to G than to RG, thereby favoring the uncoupled state. The model therefore implies that the heterogeneity revealed by agonists is induced by the G protein in an otherwise homogeneous population of mutually independent sites. Such schemes have been used extensively to rationalize the biochemical and pharmacological properties of G protein-coupled receptors (*2*, *13* and refs cited therein), but they have failed to account quantitatively for the binding of agonists (*13*−*16*). They also are at variance with evidence that the RG complex is neither transient nor destabilized by guanyl nucleotides (*17*−*21*).

An alternative view is based on the notion of an oligomeric receptor that interconverts spontaneously between two states that differ in their cooperative properties (*6*). According to that view, the signaling complex comprises multiple equivalents of both the receptor and the G protein. The different states of affinity revealed by agonists derive from cooperativity in the binding of ligands to interacting receptors (*6*, *17*); similarly, the different states of affinity revealed by GDP[1] in similar studies with [^{35}S]GTPγS derive from cooperativity in the binding of guanyl nucleotides to interacting G proteins (*22*). Guanyl nucleotides act allosterically to modulate cooperativity in the binding of agonists, and agonists are allosteric modulators of cooperativity in the

† This work was supported by the Heart and Stroke Foundation of Ontario (T4914, T5650) and the Canadian Institutes of Health Research (MOP 43990).

* To whom correspondence should be addressed. Leslie Dan Faculty of Pharmacy, University of Toronto, 144 College Street, Toronto, Ontario M5S 3M2, Canada. Tel: (416) 978-3068. Fax: (416) 978-8511. E-mail: jwells@phm.utoronto.ca.

10.1021/bi6026105 CCC: $37.00
Published on Web 06/07/2007

binding of guanyl nucleotides (*6*). Questions that arise from such a scheme relate to the nature and determinants of oligomerization, the size and composition of the signaling complex, the existence and role of monomers, the evidence for cooperative effects, and the implied link between cooperativity and response.

Interest in the structural basis of oligomerization has focused on two modes of association, generally within dimers: domain-swapping and contact between contiguous but structurally autonomous partners. Early studies on complementary chimeras of the α_{2C}-adrenergic and M_3 muscarinic receptors suggested that a site of adrenergic or muscarinic specificity could be formed from the N- and C-terminal segments of two coexpressed chimeras (i.e., α_2/M_3 and M_3/α_2) (*23*). Later data from evolutionary comparisons (*24*), molecular dynamics simulations (*24*), site-directed mutagenesis (*25*), atomic force microscopy (*26*), and X-ray crystallography (*27*) are more consistent with contacts between preformed monomers. The latter possibility is supported by the observation that monomers of the M_2 muscarinic receptor purified from *Sf*9 cells retain their characteristic affinity for muscarinic antagonists (*28*).

Although the size of the oligomer remains unclear, studies into the mechanism of binding have suggested that the M_2 muscarinic receptor is tetrameric or larger. At least four interacting sites were required for cooperativity to account for the binding properties of a complex of muscarinic receptors and G proteins purified from porcine atria, where the effect of oxotremorine-M on the antagonist [^{3}H]AF-DX 384 was bell shaped in the presence of GMP-PNP (*17*). At least four interacting sites also were required to account for the nucleotide-sensitive binding of agonists to muscarinic receptors in membranes from hamster heart (*6*). Conversely, at least two interacting sites were required for cooperativity to account for the bell-shaped effect of GDP on the binding of [^{35}S]GTPγS to G proteins linked to cardiac muscarinic receptors, also in membranes from hamster heart (*22*). The signaling complex therefore appears to be multimeric in both receptor and G protein.

Further evidence for cooperativity at cardiac muscarinic receptors has emerged in the binding of antagonists, which have revealed noncompetitive effects under some conditions. Receptors that copurify with G proteins in digitonin−cholate or that are extracted from porcine atria in either cholate−NaCl or Lubrol-PX exhibit a shortfall in the apparent capacity for *N*-[^{3}H]methylscopolamine relative to that for [^{3}H]-quinuclidinylbenzilate (*17*, *29*). Some receptors are therefore of anomalously weak affinity for *N*-methylscopolamine, yet comparatively low concentrations of that ligand inhibit the binding of [^{3}H]quinuclidinylbenzilate at saturating concentrations of the latter. Essentially the same pattern has been described for the binding of antagonists to D_2 dopamine receptors in membranes from CHO and *Sf*9 cells (*30*, *31*). Such effects at the cardiac muscarinic receptor can be described quantitatively in terms of cooperativity among four interacting sites (*17*, *29*); in accord with that interpretation, those effects disappear when the M_2 muscarinic receptor is purified as a monomer (*28*). Evidence that speaks more directly to the size of oligomers formed by G protein-coupled receptors is inconclusive, with different studies pointing to two, four, or more components (*32*).

In the present investigation, we have sought to reassemble the multimeric heteromer that has been suggested to mediate signaling. Monomers of the M_2 muscarinic receptor have been purified from *Sf*9 cells and incorporated into phospholipid vesicles, both alone and together with G proteins. Receptors in the reconstituted preparation closely resemble those in myocardial preparations with respect to the noncompetitive binding of antagonists and the guanyl nucleotide-sensitive dispersion of affinities characteristic of agonists. The data can be described quantitatively and consistently in terms of cooperativity among four interacting sites. After chemical cross-linking, most of the reconstituted receptors exhibit the electrophoretic mobility expected of tetramers.

MATERIALS AND METHODS

Ligands, Antibodies, and Other Materials. (−)-[^{3}H]Quinuclidinylbenzilate and *N*-[^{3}H]methylscopolamine were purchased either from PerkinElmer Life Sciences ([^{3}H]QNB, lot 3499844, 42 Ci/mmol; [^{3}H]NMS, lots 3499213 and 3538031, 81 Ci/mmol) or from Amersham Biosciences ([^{3}H]-QNB, lot B49, 49 Ci/mmol; [^{3}H]NMS, lot B32A, 84 Ci/mmol). Unlabeled *N*-methylscopolamine hydrobromide, carbamoycholine chloride (carbachol), and oxotremorine-M were purchased from Sigma-Aldrich.

Holo-G proteins were purchased from Calbiochem as a mixture of functional heterotrimers (i.e., $\alpha_o\beta\gamma$ and $\alpha_{i1-3}\beta\gamma$) solubilized in HEPES buffer. Digitonin used for solubilization and purification of the receptor was purchased from Wako Bioproducts at a purity near 100%. Digitonin for the buffers used to pre-equilibrate and to elute the columns of Sephadex G-50 in binding assays was from Calbiochem. Sephadex G-50 (fine) was purchased from Sigma-Aldrich, and Fast-Flow DEAE-Sepharose was from Amersham Biosciences. Suppliers of other chemicals were as follows: ACP Chemicals (magnesium sulfate, sodium phosphate, and chloroform), BDH (magnesium chloride and sodium chloride), Bioshop Canada (EDTA and DTT), Caledon Laboratories (glycerol), EM Science (Glycine, SDS, and potassium phosphate), EMD Chemicals (methanol), Pierce (BS^3), Roche Diagnostics (HEPES), and Sigma-Aldrich (sodium cholate, Tween-20, PMSF, and Trizma base).

Econo-Pacs and Econo-Columns were purchased from Bio-Rad Laboratories, and receptor was concentrated using Centricon and Centriprep concentrators (Amicon) from Millipore. Protein concentration was estimated by means of bicinchoninic acid using the BCA Protein Assay Kit and bovine serum albumin, taken as the standard, purchased from Pierce.

[1] Abbreviations: 4-NMPB, *N*-methyl-4-piperidylbenzilate; ABT, 3-(2′-aminobenzhydryloxy)tropane; AIC_C, second-order Akaike's information criterion; BASED, *bis*[*β*-(4-azidosalicylamido)ethyl]disulfide; BS^3, *bis*(sulfosuccinimidyl)suberate; CHO, Chinese hamster ovary; CuP, copper phenanthroline; DEAE, diethylaminoethyl; DSP, dithiobis-(succinimidyl)propionate; DTT, dithiothreitol; EDTA, ethylenediaminetetraacetic acid; GDP, guanosine diphosphate; GMP-PNP, guanylylimidodiphosphate; GTPγS, guanosine 5′-*O*-[3-(*γ*-thio)triphosphate]; HA, influenza hemagglutin; HEK, human embryonic kidney; HEPES, sodium *N*-(2-hydroxyethyl)piperazine-*N*′-2-ethanesulfonate; IB, immunoblot; IP, immunoprecipitation; M_2R, M_2 muscarinic acetylcholine receptor; NK1, neurokinin-1; NMS, *N*-methylscopolamine; oxo, oxotremorine-M; PMSF, phenylmethylsulfonylfluoride; QNB, (−)-quinuclidinylbenzilate; *Sf*9, *Spodoptera frugiperda*; Tris, Tris(hydroxymethyl)aminomethine.

Peroxidase-conjugated anti-HA antibody (goat) was purchased from Roche Diagnostics. Agarose-conjugated anti-FLAG (M2, mouse) and anti-HA (goat) antibodies were obtained from Sigma-Aldrich. Ascites fluid (mouse) containing a monoclonal antibody directed against the M_2 muscarinic receptor was purchased from Affinity Bioreagents, and a polyclonal antibody (rabbit) directed against the third intracellular loop was from Chemicon.

Epitope-Tagged M_2 Muscarinic Receptor from Sf9 Cells. Human M_2 muscarinic receptor bearing the HA or FLAG epitope at the amino terminus was expressed in *Sf*9 cells as described previously (*33*). The cells were cultured at 27 °C in Ex-Cell 400 insect media (JRH Biosciences) containing 2% fetal bovine serum, 1% Fungizone, and 0.1% gentamycin (all from Gibco-BRL). Cells growing at a density of 2×10^6 cells/mL were infected with baculovirus for one or both epitope-tagged receptors at a total multiplicity of infection of 5. Cells were collected by centrifugation (1000*g*) 48 h after infection, resuspended in Buffer A (20 mM KH_2PO_4, 20 mM NaCl, and 1 Complete Protease Inhibitor Cocktail Tablet (Roche Diagnostics)), and solubilized in digitonin−cholate (0.86% digitonin and 0.17% cholate) as described previously (*33*). The solubilized receptor was purified by successive passage on DEAE-Sepharose, ABT−Sepharose, and hydroxyapatite. The final concentrations of digitonin and cholate were 0.1% and 0.02%, respectively. Further details regarding the purification have been described previously (*17*). Purified receptor was stored at −75 °C.

Reconstitution of Purified M_2 Muscarinic Receptor into Phospholipid Vesicles. Reconstitution was carried out essentially as described previously (*34*). Phosphatidylcholine (0.6 mg), phosphatidylserine (0.6 mg), and cholesterol (0.06 mg) (all from Sigma-Aldrich) were dissolved in chloroform and dried uniformly under argon to a thin film. The dried film was suspended in 1 mL of Buffer B (20 mM HEPES, 160 mM NaCl, 0.8 mM EDTA, and NaOH to pH 8.0) containing 0.18% deoxycholate (Sigma-Aldrich) and 0.04% sodium cholate. Purified receptor (6 pmol in 60 μL) was incubated with carbachol (10 mM in 40 μL of Buffer B) for 15 min at 4 °C, mixed with the lipid suspension (100 μL), and applied to a column of Sephadex G-50 (0.8×5.0 cm) preequilibrated with Buffer B. To disrupt the phospholipid vesicles and resolubilize the receptor after reconstitution, the mixture was supplemented with 0.86% digitonin and incubated for 2 h at 4 °C.

To reconstitute the receptor together with holo-G proteins, Buffer B was supplemented with 1 mM DTT and 6 mM $MgCl_2$. An aliquot of G proteins was added to the receptor following incubation of the latter with carbachol. The mixture was incubated for an additional 5 min at 4 °C and then was incorporated with the lipids as described above. Unless otherwise stated, G proteins were added in the ratio of 10 α-subunits per receptor.

Cross-Linking. Solubilized or reconstituted receptor was incubated with BS^3 (2 mM) for 30 min at room temperature. Controls were prepared in the same manner except that BS^3 was omitted. The reaction was terminated by adding Tris-HCl (pH 7.50) at a final concentration of 20 mM and placing the sample in an ice bath.

Immunoprecipitation, Electrophoresis, Western Blotting, and Silver Staining. Most procedures were carried out essentially as described previously (*28*, *33*). Samples were prepared for electrophoresis by heating for 5 min at 65 °C, which has been shown not to induce aggregation (*28*). Gels destined for western blotting were loaded with 3−5 ng of receptor, except in the case of immunoprecipitates as described below. The amount of receptor was estimated from the binding of [^{3}H]quinuclidinylbenzilate at a concentration of about 100 nM. The separation was carried out on precast polyacrylamide gels from Bio-Rad (Ready Gel Tris-HCl, 10%). Molecular weight standards (Bio-Rad or Amersham Biosciences) were processed in parallel under the same conditions. The relative molecular mass of bands and standards has been divided by 1000 throughout.

To test for coimmunoprecipitation, an aliquot of tagged receptor from coinfected cells (500 μL) was supplemented with a 50% slurry of the agarose-conjugated anti-FLAG or anti-HA antibody (20 μL) and shaken overnight at 4 °C. Immunoadsorbed receptor was collected by centrifugation for 5 min at 4 °C and 1000*g*, and the precipitated beads were washed four times by resuspension in 1 mL of washing buffer (9.1 mM Na_2HPO_4, 1.7 mM NaH_2PO_4, 150 mM NaCl, and NaOH to pH 7.40) and subsequent centrifugation. The entire precipitate then was applied to the gel. The amount of receptor taken for immunoprecipitation was 20-fold greater than that taken from the same sample and applied directly to the same gel for purposes of comparison.

For identification by western blotting, resolved proteins were transferred onto nitrocellulose membranes (Bio-Rad, 0.45 μm) in a Mini Trans-Blot Transfer Cell (Bio-Rad). The membranes then were treated for 2 h with the appropriate antibody at a dilution of 1:1000 and, when necessary, for 1 h with a horseradish peroxidase-conjugated secondary antibody (Amersham Biosciences) at a dilution of 1:3000. Proteins were visualized by chemiluminescence using reagents and film purchased from Amersham Biosciences (ECL, Hyperfilm MP).

Silver staining was carried out using the ProteoSilver kit from Sigma-Aldrich. Stained gels were photographed in a Transilluminator Gel Documentation System (UVP, Model M-20) equipped with an 8-bit camera. The density was quantified using ImageJ (*35*), recording across the entire width of the lane. A baseline was subtracted, and the areas of the peaks were estimated by Gaussian deconvolution using PeakFit (Systat). The peaks obtained in an initial fit were adjusted to ensure maximum overlap between the fitted trace and the densitometric scan; the intensity of each band was taken as the sum of the major peak and any minor or hidden peaks that were required to obtain a good description of the data. Densities are expressed as a percentage of the total signal from all of the bands within each lane.

Protein Identification by Mass Spectrometry. Bands were excised from silver-stained SDS−polyacrylamide gels, destained, and digested in the gel using sequencing-grade trypsin (Promega). Digested samples were pressure-loaded onto a fused silica microcapillary column packed in-house with C12 reverse-phase Jupiter material (Phenomenex). The peptides were eluted from the column using HPLC, ionized by electrospray ionization, and analyzed in an LTQ-XL ion-trap mass spectrometer (Thermo Electron Corporation). Peptide ions were selected dynamically using data-dependent acquisition by the operating software for fragmentation. The fragmentation spectra were searched against the NCBI

Scheme 1

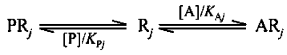

nonredundant protein database using SEQUEST on a Sorcerer platform (Sage-N Research).

Binding Assays. The radioligand and any unlabeled ligand were dissolved in Buffer C (20 mM HEPES, 20 mM NaCl, 5 mM $MgSO_4$, 1 mM EDTA, 0.1 mM PMSF, and NaOH to pH 7.40); for assays of solubilized receptor, Buffer C was supplemented with 0.1% digitonin and 0.02% cholate. An aliquot of the ligand-containing solution (50 μL) was added to the solubilized or reconstituted receptor (3 μL) in polypropylene microcentrifuge tubes. The reaction mixture was incubated at 30 °C for 2 h in the case of [^{3}H]-quinuclidinylbenzilate and for 45 min in the case of *N*-[^{3}H]-methylscopolamine. Nonspecific binding was taken throughout as total binding in the presence of 1 mM unlabeled *N*-methylscopolamine. Bound radioligand was separated by applying an aliquot of the sample (50 μL) to a column of Sephadex G-50 fine (0.8 × 6.5 cm) pre-equilibrated with Buffer D (20 mM HEPES, 20 mM NaCl, 5 mM $MgSO_4$, 1 mM EDTA, and NaOH to pH 7.40) supplemented with 0.017% digitonin. All of the eluant up to and including the void volume was collected (1.60 mL) and assayed for radioactivity (*29*).

Analysis of Data and Statistical Procedures. All data were analyzed with total binding taken as the dependent variable (B_{obsd}) and with the total concentrations of all ligands taken as the independent variables. The values listed for total receptor ($[R]_t$ or $[RT]_t$), maximal specific binding (B_{max}), and the concentrations of ligands are the concentrations in the binding assays.

Data acquired at graded concentrations of [^{3}H]quinuclidinylbenzilate or *N*-[^{3}H]methylscopolamine were analyzed empirically according to the Hill equation, formulated as shown in eq 1.

$$B_{obsd} = B_{max}\frac{([P]_t - B_{sp})^{n_H}}{EC_{50}^{n_H} + ([P]_t - B_{sp})^{n_H}} + NS\,([P]_t - B_{sp}) \quad (1)$$

The parameter B_{max} represents maximal specific binding of the radioligand (P), and B_{sp} represents specific binding at the total concentration $[P]_t$. The parameter EC_{50} represents the concentration of unbound radioligand that corresponds to half-maximal specific binding, and n_H is the Hill coefficient. The parameter NS represents the fraction of unbound radioligand that appears as nonspecific binding, which was found to increase linearly with the concentration of unbound [^{3}H]quinuclidinylbenzilate or *N*-[^{3}H]methylscopolamine. Equation 1 was solved numerically (*36*).

For data acquired at a single concentration of [^{3}H]-quinuclidinylbenzilate and graded concentrations of unlabeled *N*-methylscopolamine or oxotremorine-M, the Hill equation was formulated as $B_{obsd} = (B_{[A]=0} - B_{[A]\to\infty})EC_{50}^{n_H}/(EC_{50}^{n_H} + [A]_t^{n_H}) + B_{[A]\to\infty}$. The variable $[A]_t$ is the total concentration of unlabeled ligand, and the parameters $B_{[A]=0}$ and $B_{[A]\to\infty}$ represent the asymptotic levels of binding when $[A]_t = 0$ and as $[A]_t \to \infty$.

Mechanistic analyses were performed in terms of intrinsic heterogeneity (Scheme 1) and cooperativity (Schemes 2 and 3). Estimates of total binding were fitted by the equation $B_{obsd} = B_{sp} + NS([P]_t - B_{sp})$, in which the variables and parameters are as described above for eq 1. The value of B_{sp} was computed according to Scheme 1, 2, or 3, as described below.

Scheme 2

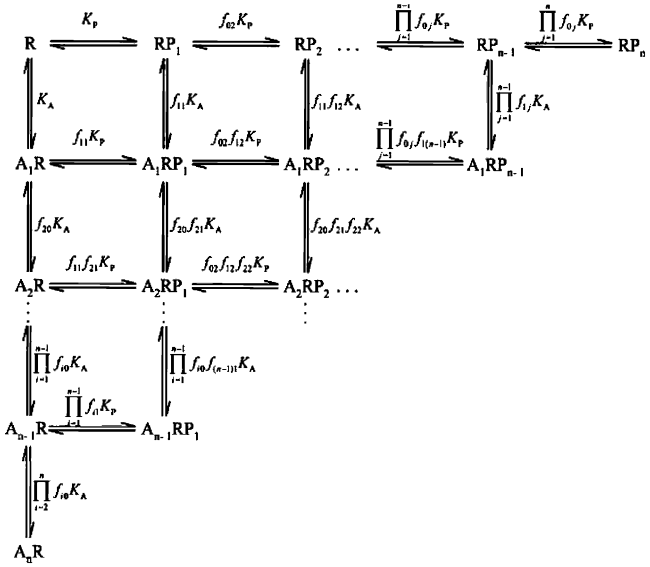

Scheme 3

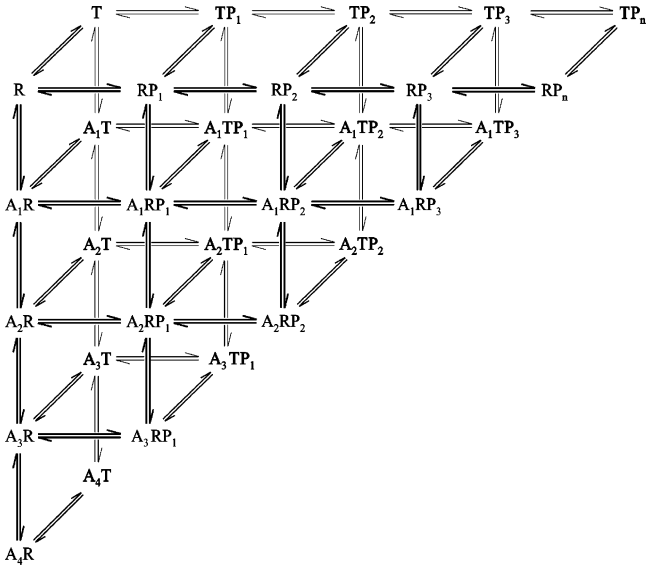

Scheme 1 represents an intrinsically heterogeneous system in which the radioligand (P) and an unlabeled ligand (A) compete for distinct and mutually independent sites (R_j, j = 1, 2, ..., n). Sites of type j bind P and A with equilibrium dissociation constants K_{Pj} and K_{Aj}, respectively, and constitute the fraction F_j of all sites (i.e., $F_j = [R_j]_t/[R]_t$, where $[R_j]_t = [R_j] + [AR_j] + [PR_j]$, and $[R]_t = \sum_{j=1}^{n}[R_j]_t$). Total specific binding of the probe was calculated according to eq 2, and the required values of $[PR_j]$ were obtained as described below.

$$B_{sp} = \sum_{j=1}^{n}[PR_j] \quad (2)$$

Cooperativity was modeled according to Scheme 2 or Scheme 3, in which a multivalent receptor can bind up to *n*

equivalents of either A or P. The receptor presumably is an oligomer, and it is assumed in each case that the oligomeric status remains unchanged under the conditions of the binding assays. There can be no exchange of subunits within the system, although the models can accommodate processes in which dissociated monomers regroup without exchanging partners.

In the case of Scheme 2, the vacant receptor exists in a single state designated R. Asymmetry cannot be detected with the present data, and all of the sites are assumed to bind P or A with the microscopic dissociation constant K_P or K_A, respectively (e.g., $K_P = [P][R]/[PR]$). Similarly, the microscopic dissociation constant was taken to be the same for all vacant sites on the partially liganded receptor (e.g., $[P][POOA]/[PPOA] = [P][POOA]/[POPA]$, where O represents a vacant site on a tetravalent receptor). The parameters f_{i0} and f_{0j} represent the cooperativity factors for the binding of the ith equivalent of A ($i \geq 2$) or the jth equivalent of P ($j \geq 2$) to form A_iR or RP_j, respectively (e.g., $[RP_{j-1}][P]/[RP_j] = \Pi_{k=2}^{j} f_{0k}K_P$). The parameters f_{ij} represent cooperativity factors in the formation of mixed complexes (i.e., A_iRP_j). Either form of cooperativity may be positive ($f < 1$) or negative ($f > 1$). The value of f_{00}, f_{10}, and f_{01} is defined as 1 in each case. Total specific binding of the probe was calculated according to eq 3.

$$B_{sp} = \sum_{j=1}^{n}\sum_{i=0}^{n-j} j\binom{n}{j}\binom{n-j}{i}[A_iRP_j] \quad (3)$$

Scheme 3 is an extension of Scheme 2 in which the receptor interconverts spontaneously between two states designated R and T. The distribution of the vacant receptor between the two states at equilibrium is given by K_{RT} (i.e., $R \rightleftharpoons T$, where $[R]/[T] = K_{RT}$). The total concentration of receptor is the sum of the vacant and all liganded forms in both states, and that quantity is represented as $[RT]_t$ (i.e., $[RT]_t = [R]_t + [T]_t$). The parameters associated with the binding of P or A are analogous to those of Scheme 2, with a separate set for each state (i.e., K_{PR}, K_{PT}, K_{AR}, K_{AT}, f_{Ri0}, f_{Ti0}, f_{R0j}, f_{T0j}, f_{Rij}, and f_{Tij}). Similarly, assumptions regarding symmetry are the same as those in Scheme 2. Total specific binding was calculated according to eq 4.

$$B_{sp} = \sum_{j=1}^{n}\sum_{i=0}^{n-j} j\binom{n}{j}\binom{n-j}{i}[A_iRP_j] + \sum_{j=1}^{n}\sum_{i=0}^{n-j} j\binom{n}{j}\binom{n-j}{i}[A_iTP_j] \quad (4)$$

The values of $[PR_j]$ in eq 2, $[A_iRP_j]$ in eq 3, and $[A_iRP_j]$ and $[A_iTP_j]$ in eq 4 were calculated from the expansions in terms of the free concentrations of A and P (i.e., [A], [P]) and the total concentrations of receptor (i.e., $[R_j]_t$ in Scheme 1, $[R]_t$ in Scheme 2, and $[R]_t$ and $[T]_t$ in Scheme 3). The values of [A] and [P] were computed numerically from the corresponding implicit equations for $[A]_t$ and $[P]_t$. This latter process requires intermediate estimates of the concentration of vacant receptor, which were calculated from the equation of state for the receptor expanded in terms of [A] and [P]. In the case of Scheme 3, those values were calculated from the equations $[R] = [RT]_t K_{RT}/(\varphi_R K_{RT} + \varphi_T)$ and $[T] = [RT]_t/(\varphi_R K_{RT} + \varphi_T)$, where φ_R and φ_T represent the first derivatives with respect to [R] and [T] of the expanded equations of state for $[R]_t$ and $[T]_t$, respectively. Further details regarding the numerical procedures have been described elsewhere (*6*, *36*).

In some analyses with Scheme 1, the model was applied in an empirical manner to obtain a good approximation of the data at the expense of mechanistic consistency (Tables 2 and 4, and Figures 4 and 10). In such cases, P and A represent the radioligand (i.e., [^{3}H]quinuclidinylbenzilate or *N*-[^{3}H]methylscopolamine) and the unlabeled ligand (*N*-methylscopolamine), respectively. Schemes 1−3 otherwise were applied in a mechanistically consistent manner, as enforced through the assignment of parameters among the different sets of data (Tables 3 and 5, and Figures 6, 7, and 11). In those cases, K_{Pj} (Scheme 1), K_P (Scheme 2), and K_{PR} (Scheme 3) denote the affinity of [^{3}H]quinuclidinylbenzilate, and K_{Aj}, K_A, and K_{AR} denote the affinity of both labeled and unlabeled *N*-methylscopolamine. The factor f_{0j} in Scheme 2 denotes cooperativity between successive equivalents of [^{3}H]-quinuclidinylbenzilate, and f_{i0} denotes cooperativity between successive equivalents of either labeled or unlabeled *N*-methylscopolamine; the factor f_{ij} ($i \neq 0$, $j \neq 0$) refers to the interaction between [^{3}H]quinuclidinylbenzilate and *N*-methylscopolamine. Likewise, the factors f_{Ri0}, f_{Ti0}, f_{R0j}, f_{T0j}, f_{Rij}, and f_{Tij} denote the corresponding modes of cooperativity in Scheme 3.

Equilibrium dissociation constants and cooperativity factors were optimized throughout on a logarithmic scale (i.e., $\log K_{Pj}$, $\log K_{Aj}$, $\log K_{RT}$, $\log f_{ij}$, etc.). Some values of f were undefined in Scheme 3 and at higher values of n in Scheme 2, and the number of parameters therefore was reduced to achieve a minimum in the sum of squares. In some cases, two or more cooperativity factors shared a single parametric value; in others, an unknown parameter was fixed at a value determined by mapping. Nonspecific binding was close to zero in assays at graded concentrations of *N*-methylscopolamine or oxotremorine-M, and the fitted estimates of NS tended to be below the precision of a floating point variable. Those values of NS therefore were determined from empirical analyses in terms of Scheme 1 and were fixed accordingly in all subsequent analyses in terms of Schemes 1−3 when the model was applied in a mechanistically consistent manner.

Most analyses involved multiple sets of data, and specific details regarding the assignment of shared parameters are described where appropriate. Values of NS and either $[R]_t$ or $[RT]_t$ were assigned separately to data from separate experiments. Except where stated otherwise, a single value of $[R]_t$ was assigned to *N*-[^{3}H]methylscopolamine and [^{3}H]-quinuclidinylbenzilate when the data were acquired in parallel; similarly, a single value was assigned to all of the data acquired at two concentrations of [^{3}H]quinuclidinylbenzilate and graded concentrations of an unlabeled ligand. The results of analyses involving multiple sets of data from replicated experiments have been presented in each case with reference to a single fitted curve. To obtain the values plotted on the *y*-axis, estimates of B_{obsd} were adjusted according to the equation $B'_{obsd} = B_{obsd} f(\bar{\mathbf{x}}_i, \bar{\mathbf{a}})/f(\mathbf{x}_i, \mathbf{a})$ as described previously (*22*).

Parametric values were estimated throughout by nonlinear regression. Fits of Schemes 2 and 3 at different values of n

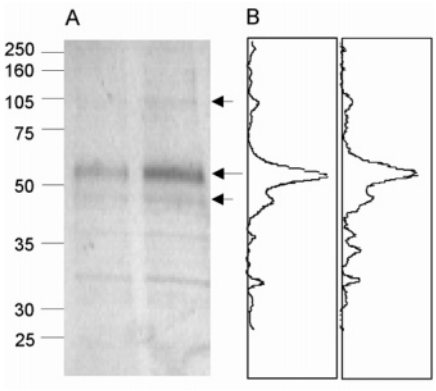

FIGURE 1: Purity of M_2 receptor recovered from DEAE-Sepharose, ABT-Sepharose, and hydroxyapatite. Aliquots of the purified preparation were concentrated and applied to the polyacrylamide gel, where the resolved bands were detected by silver staining (A) and quantified by densitometry (B). The left- and right-hand lanes in panel A received 29 and 58 ng of receptor, respectively, to yield the corresponding traces in panel B. The amount of receptor was estimated from the binding of [^{3}H]QNB at a concentration of 117 nM. The data are representative of the results from three different preparations of purified receptor.

were compared by means of Akaike's Information Criterion (AIC_C), which can be used to assess the benefit of additional parameters in nested and non-nested models (*37*). Further details regarding the analyses and related procedures have been described elsewhere (*6*, *22*, *36*).

RESULTS

Direct Identification of Oligomers. HA- and FLAG-tagged M_2 muscarinic receptors were coexpressed in *Sf*9 cells and purified by successive passage on DEAE-Sepharose, ABT-Sepharose, and hydroxyapatite. The major band detected after electrophoresis and silver staining migrated as expected for a monomer of the M_2 receptor (Figure 1A, long arrow) and represented 60−70% of the total signal from the gel (Figure 1B). Two of the minor bands migrated as a dimer (M_r ~105) and what may be an unglycosylated monomer (M_r ~48) (*38*) (Figure 1A, short arrows), and each accounted for 5−10% of the total signal (Figure 1B). The electrophoretic pattern was essentially the same over a 2-fold range of receptor applied to the gel. The three bands identified by arrows in Figure 1 therefore represent at least 70% of the protein, as revealed by silver staining, and all were shown by mass spectrometry to yield tryptic fragments of the M_2 muscarinic receptor. Other bands generally were of lower mass, including one that may be a proteolytic fragment of the receptor (M_r ~32), and each accounted for less than 10% of the total signal (Figure 1B).

The receptor was recovered primarily in monomeric form, as described previously (*28*). Immunoreactive material identified on western blots generally migrated either as a single band ($M_r = 60 \pm 1$, $N = 4$) (Figure 2A, lane 1; Figure 2D, lane 2) or as a doublet ($M_r = 49 \pm 1$, 59 ± 2, $N = 9$); some preparations also showed a comparatively faint band with the mobility of a dimer. There was a close correspondence between the bands on western blots and those identified by the arrows in Figure 1. The monomeric status implied by the electrophoretic mobility of the purified receptor was confirmed by the failure of the cross-linking reagent BS^3 to slow the migration of more than a minor

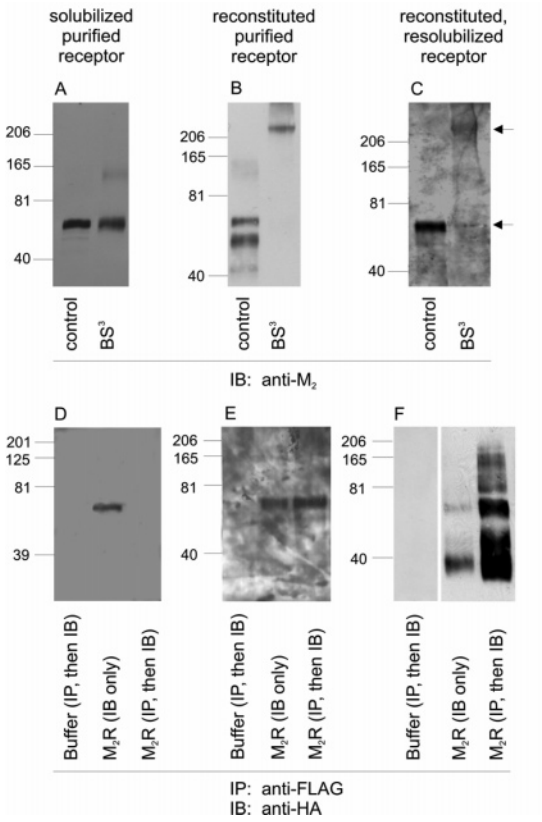

FIGURE 2: Cross-linking and coimmunoprecipitation of the purified M_2 muscarinic receptor. Samples of the tagged receptor purified from coinfected *Sf*9 cells (HA-M_2 and FLAG-M_2) were taken after recovery from hydroxyapatite (A and D), after subsequent reconstitution (B and E), and after dissolution of the reconstituted material in 0.86% digitonin (C and F). The samples shown in panels A−C were incubated in the absence of cross-linker (lanes 1) and in the presence of 2 mM BS^3 (lanes 2) before being applied to the gel, and the transferred material was blotted with the monoclonal anti-M_2 antibody. Those shown in panels D−F were mixed with the immobilized anti-FLAG antibody, and the precipitate was applied to the gel; the transferred material was blotted with the anti-HA antibody (lanes 3). Samples lacking the receptor but otherwise identical to those described above were processed in parallel (lanes 1). A sample of the purified receptor was applied directly to the gel and blotted subsequently with the anti-HA antibody (lanes 2). The sample in lane 1 of panel F and those in lanes 2 and 3 are from different experiments; the former result is typical of several such blots with the same batch of antibody. Bands corresponding to a relative molecular mass of less than 40 were observed on some occasions (e.g., panel F, lanes 2 and 3) and likely correspond to receptor that had been cleaved within the third intracellular loop. Such bands generally were avoided by using a sufficient amount of Complete Protease Inhibitor at the time of harvest (1 tablet per 50 mL of *Sf*9 cells).

fraction of the immunoreactive material (Figure 2A, lane 2) and by the absence of coimmunoprecipitation (Figure 2D, lane 3).

Receptor that was reconstituted into phospholipid vesicles and applied directly to the polyacrylamide gel migrated as a monomer (singlet, $M_r = 68 \pm 3$, $N = 4$; doublet, $M_r = 51 \pm 1$ and 61 ± 1, $N = 18$) (Figure 2B, lane 1; Figure 2E, lane 2). In contrast, receptor that was reconstituted and then cross-linked with BS^3 migrated almost exclusively as an oligomer equivalent in size to about four of the monomeric units ($M_r = 271 \pm 8$, $N = 7$) (Figure 2B, lane 2). The reconstituted receptor gave a positive signal when immunoprecipitated with an anti-FLAG antibody and blotted with

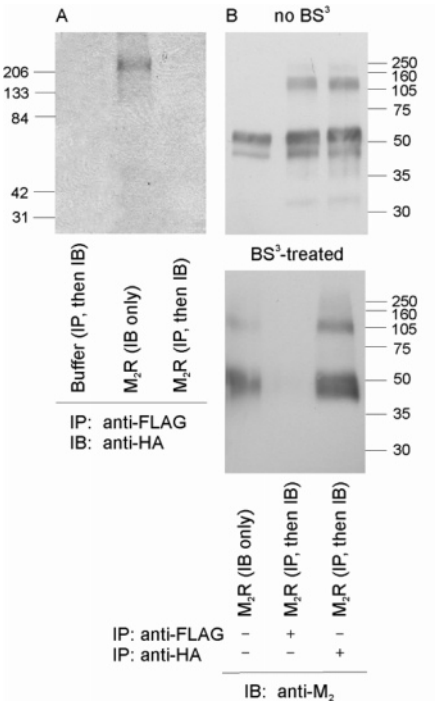

FIGURE 3: Effect of cross-linking on binding of the FLAG-tagged receptor to the immobilized anti-FLAG antibody. (A) Tagged M_2 receptor purified from coinfected cells was reconstituted into phospholipid vesicles and treated with BS^3. One aliquot was applied directly to the gel (lane 2); another was incubated first with the immobilized anti-FLAG antibody, and the precipitate was applied to the gel (lane 3). A sample lacking the receptor was incubated with the immobilized antibody in the same manner and applied to the gel (lane 1). The transferred material was blotted with the anti-HA antibody. (B) Tagged receptors purified from coinfected cells were incubated in solution in the absence of cross-linker (upper panel) or in the presence of BS^3 (lower panel). One aliquot of each sample was applied directly to the gel (lane 1); two others were mixed with either the immobilized anti-FLAG antibody (lane 2) or the immobilized anti-HA antibody (lane 3), and the precipitates were applied to the gel. The transferred material was blotted with the polyclonal anti-M_2 antibody. Both parts of panel B are from the same gel, but the exposure was longer for the cross-linked receptor.

an anti-HA antibody (Figure 2E, lane 3), a result that is consistent with the existence of oligomers but could derive from colocalization of monomers within the same vesicle.

No coimmunoprecipitation was detected with reconstituted M_2 receptor that had been treated with BS^3 (Figure 3A, lane 3), which appears to block the interaction with the anti-FLAG antibody. Untreated receptor in solution was precipitated by antibodies to either the HA or the FLAG epitope; in contrast, treatment with BS^3 eliminated precipitation by the anti-FLAG antibody without affecting that by the anti-HA antibody (Figure 3B).

Phospholipid vesicles containing the reconstituted receptor were solubilized in 0.86% digitonin to recreate the conditions of purified receptor in solution. Disruption of the vesicles was confirmed by electron microscopy. The receptor recovered from this procedure migrated largely as a tetramer if the resolubilized material was treated with BS^3 ($M_r = 232 \pm 5$, $N = 3$) (Figure 2C, lane 2). It migrated as a monomer if BS^3 was omitted (singlet, $M_r = 62 \pm 2$, $N = 3$; doublet, $M_r = 53 \pm 1$ and 63 ± 2, $N = 3$) (Figure 2C, lane 1; Figure 2F, lane 2), but the HA- and FLAG-tagged forms were found to undergo coimmunoprecipitation nonetheless (Figure 2F, lane 3). Thus, oligomers of the M_2 receptor that are formed from monomers upon reconstitution are sufficiently stable to survive solubilization in digitonin−cholate.

Effect of Reconstitution on the Binding of Antagonists, Assessed Empirically in Terms of the Hill Equation and Scheme 1. In accord with previous results (*28*), purified M_2 receptor solubilized in digitonin−cholate bound antagonists in a manner typical of a homogeneous population of monomers. The capacity for [^{3}H]quinuclidinylbenzilate and *N*-[^{3}H]methylscopolamine was the same, and the Hill coefficient in each case was near 1 (Table 1, Figure 4A). Similarly, the specific binding of [^{3}H]quinuclidinylbenzilate at saturating and subsaturating concentrations of the radioligand was inhibited fully by unlabeled *N*-methylscopolamine, and the Hill coefficient in each case was indistinguishable from 1 (Table 1, Figure 4B).

Upon reconstitution of the purified receptor into phospholipid vesicles, the apparent capacity for *N*-[^{3}H]methylscopolamine was only 60% of that for [^{3}H]quinuclidinylbenzilate, as estimated in terms of the Hill equation (Table 1; cf. Figure 4C). The shortfall was the same with *N*-[^{3}H]-methylscopolamine purchased from either PerkinElmer Life Sciences or Amersham Biosciences (cf. ref *39*), and it has been shown previously not to arise from the dissociation of *N*-[^{3}H]methylscopolamine during separation of the complex on Sephadex G-50 (*29*). Although a reduced capacity for *N*-[^{3}H]methylscopolamine can arise from a thermally unstable state of the unliganded receptor (*40*), there was no such loss in the present investigation: with the reconstituted receptor, the binding pattern obtained for *N*-[^{3}H]methylscopolamine was superimposable after incubation of the reaction mixture for 15 and 45 min. Reconstitution therefore prevented the time-dependent loss of sites for *N*-[^{3}H]methylscopolamine that otherwise can occur under some conditions. The specific binding of [^{3}H]quinuclidinylbenzilate at saturating concentrations of the radioligand was inhibited by unlabeled *N*-methylscopolamine in a monophasic manner at comparatively low concentrations of the latter (Figure 4D). Reconstitution therefore introduced heterogeneity into an otherwise homogeneous population of receptors, and unlabeled *N*-methylscopolamine appeared to inhibit the binding of [^{3}H]-quinuclidinylbenzilate at sites that were inaccessible to the former.

To examine the implications of the binding properties, the data represented in Figure 4 were analyzed in terms of Scheme 1. The fitted curves are shown in the figure, and the parametric values are listed in Table 2. In each case, the analysis included all of the data represented in the corresponding left- and right-hand panels of Figure 4. The affinity of *N*-methylscopolamine was estimated separately for the radioligand (left-hand panels) and for the unlabeled analogue at each concentration of [^{3}H]quinuclidinylbenzilate (right-hand panels). If Scheme 1 indeed describes the system, then the three estimates of log K_{Lj} for *N*-methylscopolamine at each class of sites are expected to be the same. The affinity of [^{3}H]quinuclidinylbenzilate was taken to be the same for all of the data, although values of log K_{Lj} are defined independently by the data in each panel. This constraint is consistent with the model and facilitates a comparison of the different estimates of K_{Lj} for *N*-methylscopolamine. It had no discernible effect on the fitted curves.

Table 1: Empirical Characterization of Specific Binding to the Purified M_2 Receptor[a]

preparation ligands		G protein	GMP-PNP	[[^{3}H]QNB] (nM)	log EC_{50} or log IC_{50}	n_H	$B_{max,[^3H]NMS}/B_{max,[^3H]QNB}$
solution							
[^{3}H]NMS	(3)	−	−		-7.69 ± 0.05	0.86 ± 0.07	1.02 ± 0.01
[^{3}H]QNB	(3)	−	−		-8.72 ± 0.06	0.97 ± 0.20	
NMS/[^{3}H]QNB	(3)	−	−	0.88 ± 0.03	-7.78 ± 0.10	1.34 ± 0.18	
NMS/[^{3}H]QNB	(3)	−	−	26 ± 1	-6.46 ± 0.04	1.07 ± 0.23	
oxo/[^{3}H]QNB	(3)	−	−	2.41 ± 0.03	-3.13 ± 0.12	1.03 ± 0.13	
oxo/[^{3}H]QNB	(3)	+	−	2.4 ± 0.3	-3.23 ± 0.09	0.88 ± 0.09	
oxo/[^{3}H]QNB	(3)	+	+	2.4 ± 0.3	-3.26 ± 0.13	1.03 ± 0.04	
reconstitution							
[^{3}H]NMS	(3)	−	−		-7.81 ± 0.06	0.91 ± 0.03	0.63 ± 0.04
[^{3}H]QNB	(3)	−	−		-9.16 ± 0.04	1.08 ± 0.07	
NMS/[^{3}H]QNB	(3)	−	−	0.86 ± 0.03	-7.44 ± 0.10	0.97 ± 0.10	
NMS/[^{3}H]QNB	(3)	−	−	27 ± 1	-6.03 ± 0.01	1.32 ± 0.11	
oxo/[^{3}H]QNB	(3)	−	−	2.1 ± 0.2	-3.38 ± 0.07	1.45 ± 0.31	
oxo/[^{3}H]QNB	(7)	+	−	2.1 ± 0.2	-4.40 ± 0.26	0.42 ± 0.04	
oxo/[^{3}H]QNB	(3)	+	+	2.4 ± 0.3	-3.33 ± 0.05	0.66 ± 0.13	

[a] Total binding was measured at graded concentrations of [^{3}H]NMS and [^{3}H]QNB, taken in parallel, and at graded concentrations of unlabeled NMS or oxo at a constant concentration of [^{3}H]QNB (NMS/[^{3}H]QNB, oxo/[^{3}H]QNB). Assays were performed on the receptor alone and supplemented with G proteins. Binding in the presence of G proteins was measured in the absence of guanyl nucleotide and in the presence of 0.1 mM GMP-PNP. The number of sets of data is shown in parentheses. Each set of data was analyzed independently in terms of the Hill equation, and the individual estimates of log EC_{50}, log IC_{50}, and n_H were averaged to obtained the means (±S.E.M.) listed in the table. The relative capacity for [^{3}H]NMS and [^{3}H]QNB was calculated from parallel estimates of B_{max} (i.e., $B_{max,[^3H]NMS}/B_{max,[^3H]QNB}$), and the individual values were averaged to obtain the means (±S.E.M.) listed in the table.

One class of sites is sufficient to describe binding to the purified receptor in solution (Figure 4A and B), and the affinity estimated for radiolabeled *N*-methylscopolamine (log K_{P1}) is in good agreement with that inferred for the unlabeled analogue (log K_{A1}) at either concentration of [^{3}H]quinuclidinylbenzilate (Table 2). This consistency is confirmed by the negligible effect on the weighted sum of squares when *N*-methylscopolamine is assigned a single value of K_L rather than separate values for the radiolabeled form of the ligand and for the unlabeled form at each concentration of [^{3}H]-quinuclidinylbenzilate ($P = 0.09$). It follows that *N*-methylscopolamine and quinuclidinylbenzilate bind in an apparently competitive manner to a homogeneous population of mutually independent sites.

Two classes of sites are required to describe the binding properties of the reconstituted receptor ($P < 0.00001$) (Figure 4C and D). About 50% of the sites were of anomalously weak affinity for *N*-[^{3}H]methylscopolamine (log $K_{P2} = -6.07$, Table 2), whereas the affinity of unlabeled *N*-methylscopolamine for the same sites was about 30-fold higher (log $K_{A2} = -7.60$, Table 2). At the sites of higher affinity, the two values of log K_{A1} estimated for unlabeled *N*-methylscopolamine differ almost 10-fold from each other and bracket the corresponding value estimated for the radioligand. Such differences are inconsistent with the notion of a competition for mutually independent sites.

The difference in the affinity of reconstituted receptor for labeled and unlabeled *N*-methylscopolamine is illustrated by the dotted lines in Figure 4. The line in panel C depicts the predicted binding of *N*-[^{3}H]methylscopolamine based on the values of K_{Aj} inferred from the inhibitory effect of the unlabeled analogue at the higher concentration of [^{3}H]-quinuclidinylbenzilate (i.e., log $K_{A1} = -7.60$ and log $K_{A2} = -7.60$). Likewise, the dotted lines in panel D depict the predicted effect of unlabeled *N*-methylscopolamine based on the values of K_{Lj} estimated for the radiolabeled analogue (i.e., log $K_{P1} = -8.05$ and log $K_{P2} = -6.07$) and on the concentration of [^{3}H]quinuclidinylbenzilate.

The discrepancies in affinity are confirmed by an increase of more than 2-fold in the global sum of squares when the data represented in panels C and D are reanalyzed with the parameters assigned in a mechanistically consistent manner ($P < 0.00001$): that is, with a single value of K_{Lj} rather than three for *N*-methylscopolamine at each class of sites. The sum of squares from such an analysis is not reduced with three or four classes of sites rather than two, as illustrated by the solid bars in Figure 5. It follows that Scheme 1 is inconsistent with the data regardless of the degree of heterogeneity assumed in the model. The reconstituted receptor therefore appears to bind antagonists in a noncompetitive manner.

Effect of Reconstitution on the Binding of Antagonists, Assessed in Terms of Scheme 2. Noncompetitive interactions imply cooperativity, presumably within an oligomeric array. Data obtained with the reconstituted receptor therefore were examined in terms of Scheme 2, in which the low apparent capacity for *N*-[^{3}H]methylscopolamine can be attributed to a high degree of negative cooperativity between two successive equivalents of the radioligand. If the value of f_{i0} is sufficiently large, then the macroscopic dissociation constant for the *i*th equivalent of *N*-[^{3}H]methylscopolamine will exceed the highest concentration used in the assays. Binding therefore will be precluded, both to the *i*th site and to additional sites. The inhibitory effect of unlabeled *N*-methylscopolamine will derive in part from competition for the vacant receptor and in part from cooperativity between the unlabeled ligand and [^{3}H]quinuclidinylbenzilate (i.e., log $f_{ij} \neq 0$).

All parameters were assigned to enforce mechanistic consistency, and the number of interacting sites (n) was incremented by 1 or 2 in successive analyses until any further improvement in the fit was negligible. It is assumed in

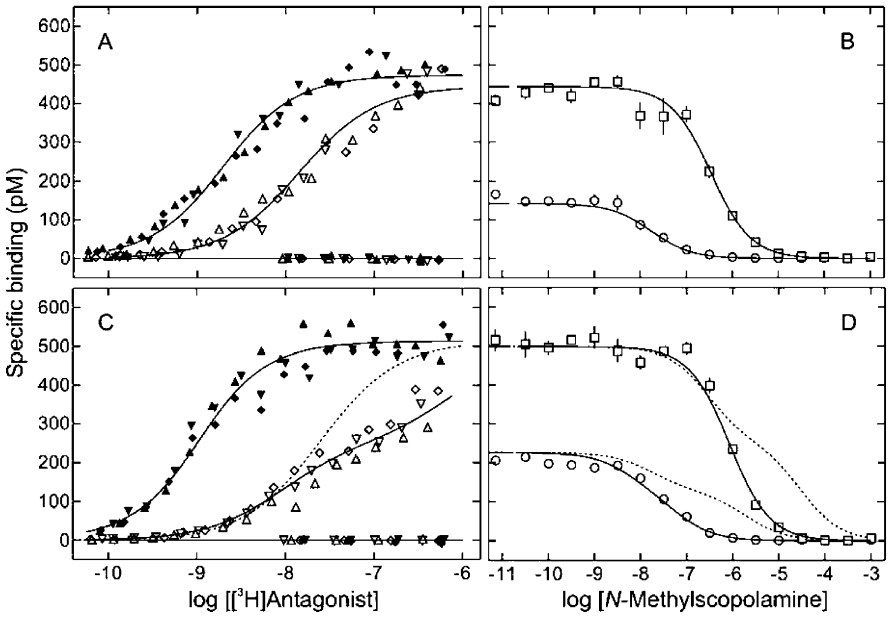

FIGURE 4: Binding of antagonists to M_2 muscarinic receptor before and after reconstitution, analyzed empirically in terms of Scheme 1. Purified receptor was assayed in solution (A and B) and after reconstitution into phospholipid vesicles (C and D). (A and C) Total binding was measured at graded concentrations of [^{3}H]QNB (▲,▼,♦) and [^{3}H]NMS (△,▽,◇), either alone (upper curves) or in the presence of 1 mM unlabeled NMS (baseline). Each experiment included assays with both radioligands taken in parallel, and different symbols denote data from different experiments (▲,△;▼,▽;♦,◇). (B and D) Total binding was measured at near-saturating (□) and subsaturating (○) concentrations of [^{3}H]QNB (B, 26 ± 1 nM and 0.88 ± 0.03 nM; D, 27 ± 1 nM and 0.86 ± 0.03 nM) and graded concentrations of unlabeled NMS (N = 3). The solid lines represent the best fits of Scheme 1 (A and B, n = 1; C and D, n = 2) to the pooled data from the six experiments represented in panels A and B and, in a separate analysis, to the pooled data from the six experiments represented in panels C and D. The value of $[R]_t$ was estimated separately for [^{3}H]QNB and [^{3}H]NMS in each experiment represented in panel A. The parametric values and further details regarding the analyses are given in Table 2. The mean values of $[R]_t$ used to obtain the adjusted values of B_{obsd} plotted on the y-axis are as follows: A and B ([^{3}H]QNB), 474 ± 21 pM, N = 9; C and D, 514 ± 61 pM, N = 7. The mean ratio of $[R]_t$ for the two radioligands in panel A is 0.94 ± 0.08 ([^{3}H]NMS/[^{3}H]QNB) (N = 3). Points shown at the lower end of the x-axis in panels B and D indicate binding in the absence of NMS. The dotted lines were simulated as described in the text and illustrate discrepancies in the affinity of NMS as estimated under different conditions.

Table 2: Parametric Values for the Binding of Quinuclidinylbenzilate and *N*-Methylscopolamine, Estimated Empirically in Terms of Scheme 1[a]

			quinuclidinylbenzilate		*N*-methylscopolamine		
preparation	L	[[^{3}H]QNB] (nM)	log K_{P1}	log K_{P2}	log K_{L1}	log K_{L2}	F_2
solution[b]	P (3)				−7.83 ± 0.02		
	A (3)	0.88 ± 0.03	−8.77 ± 0.02		−8.01 ± 0.10		
	A (3)	26 ± 1			−7.67 ± 0.05		
reconstitution	P (3)				−8.05 ± 0.06	−6.07 ± 0.16	
	A (3)[c]	0.86 ± 0.03	−9.08 ± 0.60	−9.12 ± 0.58	−8.54 ± 0.21	−7.57 ± 0.66	0.51 ± 0.04
	A (3)[c,d]	27 ± 1			−7.60 ± 0.04	−7.60 ± 0.04	

[a] The data illustrated in the paired left- and right-hand panels of Figure 4 were pooled (A and B, C and D) and analyzed according to eq 2 (n = 1 or 2) to obtain the parametric values listed in the table. QNB was present only as the radioligand (L ≡ P, both panels), whereas NMS was present either as the radioligand (L ≡ P, left-hand panel) or as the unlabeled analogue (L ≡ A, right-hand panel). The number of experiments is shown in parentheses. A single class of sites was sufficient for receptor in solution (n = 1); two classes were required after reconstitution (n = 2), and a single value of F_2 was common to all of the data. In both analyses, single values of K_{Pj} for [^{3}H]QNB were common to all of the relevant data in both panels. The model was applied empirically with respect to the treatment of K_{Pj} and K_{Aj} for labeled and unlabeled NMS; that is, separate values of K_{Aj} were assigned to the data acquired at each concentration of [^{3}H]QNB (right-hand panels), and a value of K_{Pj} was assigned to the data acquired at graded concentrations of [^{3}H]NMS (left-hand panels). [b] There is no appreciable decrease in the sum of squares with two classes of sites rather than one (P = 0.06). [c] The data acquired at different concentrations of [^{3}H]QNB in one experiment yielded appreciably different values of $[R]_t$, which therefore were optimized separately. [d] At the higher concentration of [^{3}H]QNB, the value of K_{Aj} for [^{3}H]NMS was the same at both classes of sites (i.e., $K_{A1} = K_{A2}$).

Scheme 2 that the receptor exists exclusively in the oligomeric state implied by the value of n. To investigate the possibility that those oligomers coexist with monomers, Scheme 2 was expanded to include a separate population of mutually independent sites. Oligomers and monomers were assumed not to interconvert under the conditions of the assays. The weighted sums of squares from all analyses are compared in Figure 5. The fitted curves for dimers with and without monomers are illustrated in Figure 6; those for tetramers and octamers are illustrated in Figure 7.

Each successive increase in the number of interacting sites is accompanied by a decrease in the weighted sum of squares (Figure 5). Eight interacting sites yield a fit that approximates the fit obtained from an empirical application of Scheme 1. The latter is taken here as a measure of the fit that would be obtained with the true model, were it known. Scheme 2

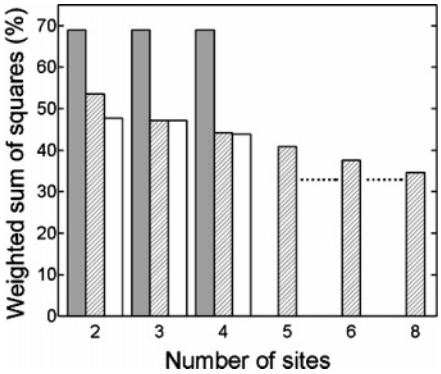

FIGURE 5: Comparison of Schemes 1 and 2 for goodness of fit to data on the binding of antagonists to reconstituted M_2 receptor. The data represented in panels C and D of Figure 4 were pooled and analyzed in terms of Schemes 1 and 2 to obtain the global sum of squares at different values of *n* (gray bars, Scheme 1; hatched bars, Scheme 2; white bars, Scheme 2 plus a separate population of mutually independent sites). The value from each analysis is plotted as a percentage of the value obtained when *n* was taken to be 1. All parameters were assigned throughout in a mechanistically consistent manner, in contrast to the empirical assignment depicted in Figure 4; thus, all relevant data shared single values of K_{Pj}, K_{Aj}, and F_j (Scheme 1), and of K_P, K_A, $K_{P(M)}$, $K_{A(M)}$, f_{0j}, f_{i0}, and f_{ij} (Scheme 2). The dashed line indicates the relative sum of squares from an unconstrained, empirical analysis in terms of Scheme 1 ($n = 2$). The fitted curves from Scheme 2 with two, four, and eight interacting sites are shown in Figures 6 and 7.

therefore differs from Scheme 1 when both models are applied in a mechanistically consistent manner: although Scheme 1 yields a marked decrease in the sum of squares when *n* is incremented from 1 to 2, there is no further improvement at higher values. It follows that Scheme 2 is tenable as a mechanistic description of the data, whereas Scheme 1 is not.

Two interacting sites reduce the sum of squares by almost 50% relative to that obtained for a single site, and the model provides at least a first approximation of the data (Figure 6A and B). Although the fit is significantly better at higher values of *n*, as described below, the parametric values for two interacting sites are well defined and offer some insight into the way in which such a model accounts for the data (Table 3). [^{3}H]Quinuclidinylbenzilate bound to all of the sites with a Hill coefficient of 1.08 (Table 1), which emerged as a comparatively small degree of positive homotropic cooperativity between the first equivalent of the radioligand and the second (i.e., $\log f_{02} = -0.44$). In contrast, *N*-[^{3}H]-methylscopolamine was restricted to 50% of the sites at lower concentrations of the radioligand (<0.1 μM) owing to negative homotropic cooperativity and a resulting 7-fold decrease in affinity between the first equivalent and the second (i.e., $\log f_{20} = 0.83$). The noncompetitive, inhibitory effect of *N*-methylscopolamine on the binding of [^{3}H]-quinuclidinylbenzilate derived from negative heterotropic cooperativity between the two ligands (i.e., $\log f_{11} = 0.45$).

Higher values of *n* improve the fit, as illustrated for a tetramer and an octamer in Figure 7. Although correlations emerge among the parameters, some of which are undefined, the overall pattern resembles that found with two interacting sites. There was little or no homotropic cooperativity between successive equivalents of [^{3}H]quinuclidinylbenzilate at any level of occupancy (i.e., $\log f_{0j} \sim 0$), whereas negative cooperativity reduced the affinity of *N*-[^{3}H]methylscopolamine for 50% of the sites. In the case of a tetramer, there was no discernible effect of the first equivalent of *N*-methylscopolamine on the binding of the second ($\log f_{20} = 0.11 \pm 0.15$) or of the third equivalent on the binding of the fourth ($\log f_{40} = 0.05 \pm 0.6$), but the microscopic dissociation constant differed 7-fold between the second equivalent and the third ($\log f_{30} = 0.85 \pm 0.30$). The noncompetitive interaction between *N*-methylscopolamine and [^{3}H]quinuclidinylbenzilate arose from a blend of negative and positive heterotropic cooperativity, depending upon the overall level of occupancy and the composition of the complex at each level (e.g., A_3R, A_2RP_1, A_1RP_2, or RP_3). The individual values of f_{ij} tend to be correlated, however, and a unique set is not defined by the present data.

The results presented in Figures 5−7 indicate that Scheme 2 can reconcile the shortfall in the apparent capacity for *N*-[^{3}H]methylscopolamine with the inhibitory effect of unlabeled *N*-methylscopolamine on the binding of [^{3}H]-quinuclidinylbenzilate. To determine the most probable size of the oligomer, the value of AIC_C was calculated for each value of *n*. There is a minimum at four interacting sites if the receptors are assumed to be exclusively oligomeric (Figure 8), and a tetrameric receptor therefore affords the most efficient description of the data. A dimer and perhaps a trimer appear to have too few parameters, whereas the additional complexity of a pentamer or a larger oligomer is not justified by the further decrease in the sum of squares. The likelihood that *n* is 4 rather than 3 or 5 is 73:27 in each case.

Since the reconstituted oligomers are assembled from monomers, some of the latter may have been incorporated as such into vesicles. The inclusion of a subclass of monomers significantly improved the fit of a dimer, as indicated by the *F*-statistic for the decrease in the sum of squares ($P = 0.00005$) and by the marked decrease in the value of AIC_C (Figure 8). The fitted curves for dimers alone and for dimers plus monomers are shown in Figure 6, and the parametric values are compared in Table 3. Monomers emerge as a minor component, however, accounting for only 6% of all sites in the augmented model. Their inclusion had little effect on the values of parameters pertaining to the dimers.

A subclass of monomers offered no improvement to the fits obtained with either a trimer or a tetramer. There was no appreciable reduction in the sum of squares ($P > 0.56$), and the value of AIC_C increased in each case (Figure 8). The value of AIC_C also was significantly lower with tetramers alone than with a mixture of dimers and monomers (90:10) (Figure 8). Taken together, the data suggest that the binding properties can be described in terms of cooperativity within a homogeneous population of tetramers.

Effect of Reconstitution on the Binding of Oxotremorine-M, Assessed Empirically in Terms of the Hill Equation and Scheme 1. The binding of oxotremorine-M was examined via its inhibitory effect on the specific binding of [^{3}H]-quinuclidinylbenzilate. Receptor in solution bound oxotremorine-M with a Hill coefficient indistinguishable from 1 ($P = 0.93$) (Table 1, Figure 9A), consistent with the notion of a homogeneous population of mutually independent sites. The Hill coefficient was somewhat higher with reconstituted receptor (Table 1, Figure 9B), but again the value was indistinguishable from 1 ($P = 0.32$).

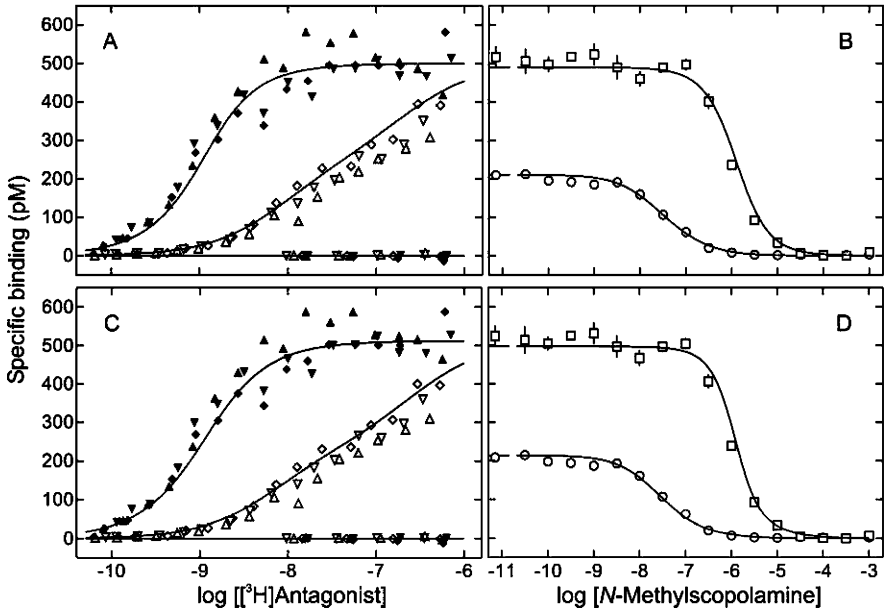

FIGURE 6: Binding of antagonists to reconstituted M_2 muscarinic receptor, analyzed in terms of Scheme 2 ($n = 2$). The data represented in panels C and D of Figure 4 were analyzed in terms of a dimer alone (A and B) and a mixture of noninterconverting dimers (R) and monomers (M) (C and D). The lines in panels A and B represent the best fit of Scheme 2 ($n = 2$) to the pooled data. The lines in panels C and D represent the best fit of a composite model that comprised Scheme 2 ($n = 2$) and the simplest variant of Scheme 1 ($n = 1$). All parameters were assigned to enforce mechanistic consistency, and the fitted values are listed in Table 3. The mean values of $n[R]_t$ and of $n[R]_t + [M]_t$ used to obtain the adjusted values of B_{obsd} plotted on the *y*-axis are 500 ± 64 pM (A and B) and 512 ± 65 pM (C and D), respectively ($N = 7$). Further details are described in the legends to Figure 4 and Table 3.

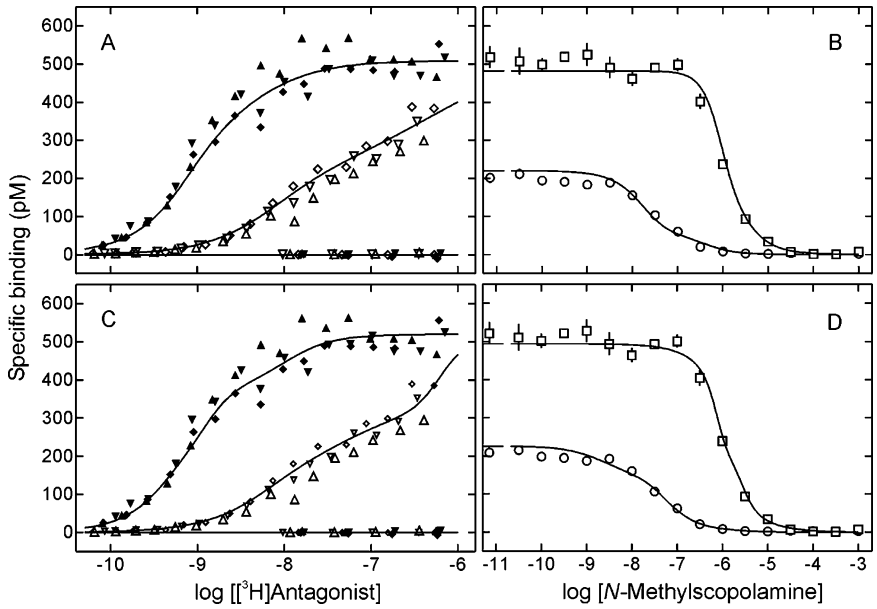

FIGURE 7: Binding of antagonists to reconstituted M_2 muscarinic receptor, analyzed in terms of Scheme 2 ($n = 4$ or 8). The data represented in panels C and D of Figure 4 were analyzed in terms of a tetramer (A and B) or an octamer (C and D). The lines represent the best fits of Scheme 2 to the pooled data with *n* taken to be 4 (A and B) and, in a separate analysis, with *n* taken to be 8 (C and D). All parameters were assigned to enforce mechanistic consistency. The mean values of $n[R]_t$ used to obtain the adjusted values of B_{obsd} plotted on the *y*-axis are 509 ± 64 pM (A and B) and 522 ± 64 pM (C and D) ($N = 7$). Further details are described in the legend to Figure 4.

To assess the binding patterns in terms of Scheme 1, the data obtained at graded concentrations of oxotremorine-M (i.e., Figure 9A and B) were pooled with those obtained at graded concentrations of [^{3}H]quinuclidinylbenzilate (i.e., Figure 4A and C) and analyzed in concert. A single class of sites was sufficient for receptors before and after reconstitution, and the fitted curves for the agonist are shown in Figure 9 (A and B). Both oxotremorine-M and [^{3}H]quinuclidinylbenzilate bound more weakly to receptor in solution (log $K_A = -3.44 \pm 0.07$ and log $K_P = -8.71 \pm 0.03$) than to the reconstituted receptor (log $K_A = -3.93 \pm 0.06$ and log $K_P = -9.16 \pm 0.02$).

Functional G proteins were essentially without effect on the binding of oxotremorine-M to the purified receptor in solution (Figure 9A and C). The Hill coefficient was marginally less than 1 ($P = 0.04$), and the inhibitory potency

Table 3: Parametric Values for the Binding of Antagonists to Reconstituted Receptor, Estimated in Terms of Scheme 2 ($n = 2$)[a]

ligand	parameter	dimer	dimer plus monomer
[^{3}H]QNB	log K_P	-8.86 ± 0.06	-8.99 ± 0.10
NMS, [^{3}H]NMS	log K_A	-7.79 ± 0.03	-7.86 ± 0.06
[^{3}H]QNB	log f_{02}	-0.44 ± 0.14	-0.13 ± 0.14
NMS, [^{3}H]NMS	log f_{20}	0.83 ± 0.08	0.98 ± 0.15
NMS/[^{3}H]QNB	log f_{11}	0.45 ± 0.13	1.36 ± 0.67
[^{3}H]QNB	log $K_{P(M)}$		-9.18 ± 0.90
NMS, [^{3}H]NMS	log $K_{A(M)}$		-6.54 ± 0.94
	F_D		0.94[b]

[a] The data illustrated in the paired left- and right-hand panels of Figure 6 were pooled (A and B, C and D) and analyzed according to eq 3 ($n = 2$) to obtain the parametric values listed in the table. For the analysis illustrated in panels C and D, the model was expanded to include a population of mutually independent sites (M), possibly monomers; the affinities of the ligands for the monomer are $K_{P(M)}$ and $K_{A(M)}$, and the supposed dimers (R) account for the fraction F_D of all sites [i.e., $F_D = 2[R]_t/(2[R]_t + [M]_t)$]. All parameters were assigned to enforce mechanistic consistency. [^{3}H]QNB was taken as ligand P, and both labeled and unlabeled NMS were taken as ligand A. Single values for K_P and f_{0j} ([^{3}H]QNB), K_A and f_{i0} (NMS, [^{3}H]NMS), and f_{ij} (NMS/[^{3}H]QNB) were common to all relevant data in both panels.[b] The value of F_D was defined by a shallow minimum in the sum of squares. It therefore was identified by mapping and fixed accordingly to obtain the fitted values listed for other parameters.

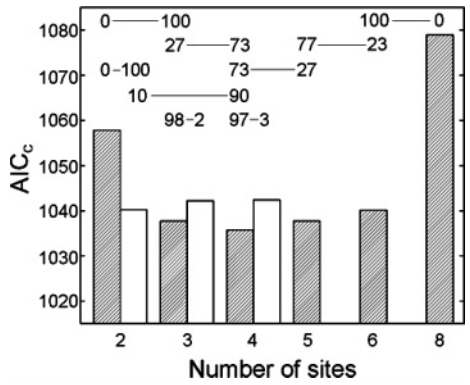

FIGURE 8: Optimal number of interacting sites for Scheme 2 to describe the binding of antagonists to reconstituted M_2 receptor. The value of AIC_C was calculated from the weighted sum of squares and the degrees of freedom at each value of n (hatched bars, oligomers alone; white bars, oligomers plus monomers). When a cooperativity factor was fixed at a specific value or when two or more cooperativity factors shared a single parametric value, the restriction was disregarded when calculating the degrees of freedom. The probability that one of two models is correct was calculated from the difference in AIC_C, and complementary estimates of P (%) are shown joined by a horizontal line above the corresponding bars.

was unchanged (Table 1). Likewise, the binding of oxotremorine-M to receptor supplemented with G proteins was unaffected by GMP-PNP (Figure 9C). Taken together, the data suggest that there was no interaction between receptor monomers and G proteins in solution.

In contrast, G proteins markedly decreased the Hill coefficient for oxotremorine-M when included with the receptor during reconstitution into phospholipid vesicles (Table 1, Figure 9D). G proteins generally were added at a ratio of 10 α-subunits per [^{3}H]quinuclidinylbenzilate-binding site, which was sufficient to saturate the receptor under the conditions of the assays. The binding patterns were superimposable when the ratio was increased to 20:1 and 30:1 (Figure 9D). The effect of G proteins on binding to the reconstituted receptor was partially reversed by GMP-PNP (Figure 10B), which increased the Hill coefficient for oxotremorine-M from 0.42 to 0.66 (Table 1).

To facilitate a comparison with previous results on the cardiac muscarinic receptor (*6*) and to obtain a baseline sum of squares, the binding of oxotremorine-M and [^{3}H]quinuclidinylbenzilate to the reconstituted mixture of receptor and G proteins was described empirically in terms of Scheme 1. The model was fitted to the data acquired with both ligands with and without GMP-PNP taken in concert. In a series of analyses, the different estimates of K_{Aj} (oxotremorine-M), K_{Pj} ([^{3}H]quinuclidinylbenzilate), and F_j were combined, where possible, to reduce the number of parameters without appreciably affecting the sum of squares ($P > 0.05$). The fitted curves from the final analysis are illustrated in Figure 10, and the parametric values are listed in Table 4.

Three classes of sites are required for oxotremorine-M in the absence of nucleotide (K_{A1}, K_{A2}, and K_{A3}), two of which were indistinguishable by [^{3}H]quinuclidinylbenzilate (i.e., $K_{P1} = K_{P2}$). GMP-PNP is seen to promote a net interconversion of sites from the state of highest affinity for the agonist (K_{A1}) to that of lowest affinity (K_{A3}), virtually eliminating the former, while having no appreciable effect on the affinity *per se* for either state. The number of sites in the state of intermediate affinity was unchanged, but there was a 6-fold increase in the value of K_{A2}. Four classes therefore are required to describe the system as a whole. The net effect of GMP-PNP was to decrease the overall affinity of the agonist (Figure 10B). GMP-PNP had a smaller but opposite effect on the binding of [^{3}H]quinuclidinylbenzilate, in that the overall affinity was higher in the presence of the nucleotide (Figure 10A).

Binding to Receptor Reconstituted with G Proteins, Assessed in Terms of Scheme 3. To account mechanistically for the effects of all ligands, the data represented in Figure 10 were reanalyzed using an extended version of Scheme 2 in which the vacant receptor interconverts spontaneously between two states (i.e., R and T). All parameters were assigned to enforce mechanistic consistency. The specific version implemented here includes four interacting sites, as shown in Scheme 3, in conformity with the level of complexity required to describe the binding of quinuclidinylbenzilate and *N*-methylscopolamine in terms of Scheme 2. An analogous scheme based on two interconverting states and only two interacting sites failed to describe the data: the sum of squares from that analysis was 1.6-fold higher than the value obtained with four interacting sites.

Scheme 3 accommodates the effects of GMP-PNP as a change in the value of K_{RT}, which defines the distribution of sites between the two states at thermodynamic equilibrium (i.e., $K_{RT} = [R]/[T]$); accordingly, changes in the binding of agonists and antagonists are attributed to differences between R and T in the affinity of the ligand for the vacant receptor or in the cooperativity factors (i.e., $K_{PR} \neq K_{PT}$, $K_{AR} \neq K_{AT}$, $f_{R0j} \neq f_{T0j}$, $f_{Ri0} \neq f_{Ti0}$, or $f_{Rij} \neq f_{Tij}$). In the present implementation, R and T represent the supposed tetramer in the absence of nucleotide and in the presence of a saturating concentration of GMP-PNP, respectively. The presence of the G protein is implicit, and the nature of its interaction with the guanyl nucleotide is undefined. The simplest assumption is that R and T denote a heterooligomer compris-

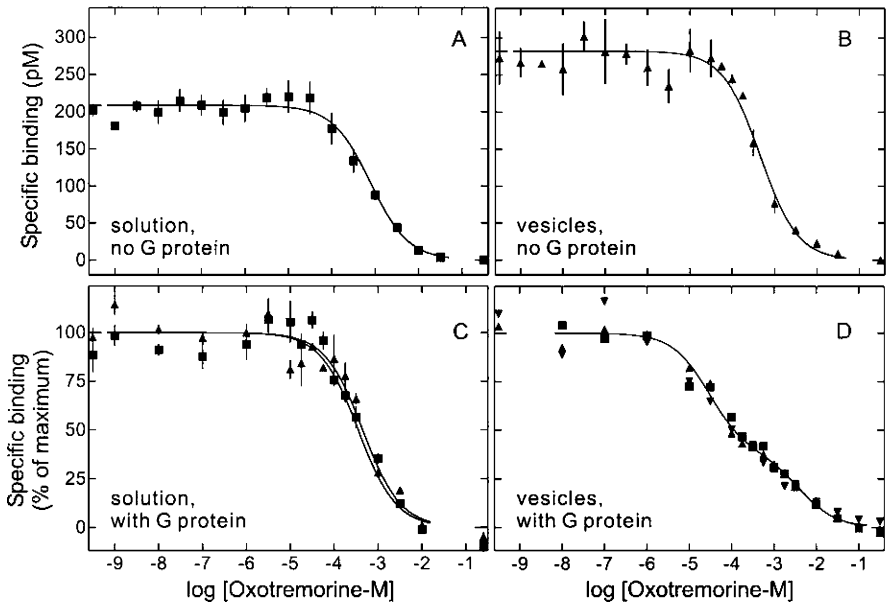

FIGURE 9: Binding of oxotremorine-M to M_2 muscarinic receptor before and after reconstitution. Purified receptor was assayed in solution (A and C) and after reconstitution into phospholipid vesicles (B and D) in the absence (A and B) and presence (C and D) of heterotrimeric G proteins. Total binding was measured at a half-saturating concentration of [^{3}H]QNB (A, 2.41 ± 0.03 nM, $N = 3$; B, 2.1 ± 0.2 nM, $N = 3$; C, 2.4 ± 0.3 nM, $N = 3$; D, 2.00 ± 0.03 nM, $N = 3$) and graded concentrations of the agonist oxo. (A and B) The lines represent the best fits of Scheme 1 ($n = 1$) to the data represented in the figure taken together with those obtained at graded concentrations of [^{3}H]QNB under the same conditions (i.e., Figure 4A and C, respectively). The fitted parametric values (i.e., K_A and K_P) are listed in the text, and the mean values of $[R]_t$ used to obtain the adjusted values of B_{obsd} plotted on the *y*-axis are as follows: A, 425 ± 44 pM, $N = 6$; B, 391 ± 76 pM, $N = 6$. (C) Purified receptor was mixed in solution with holo-G proteins at a ratio of 10 α-subunits per receptor, and binding was measured in the absence of guanyl nucleotide (▲) and in the presence of 0.1 mM GMP-PNP (■). The lines represent the best fits of the Hill equation with single values of EC_{50} and n_H for the three sets of data included in each analysis; values of $B_{[A]=0}$ and $B_{[A]\to\infty}$ were assigned separately to each set of data. The value of n_H was indistinguishable from 1 in each case and was fixed accordingly. The fitted values of EC_{50} are as follows: no GMP-PNP, log $IC_{50} = -3.35 \pm 0.05$; 0.1 mM GMP-PNP, log $IC_{50} = -3.45 \pm 0.64$. (D) Purified receptor was reconstituted with G proteins at different ratios of α-subunits to receptor (▲, 10:1; ■, 20:1; ▼, 30:1), and the results are from one of two such experiments. The line represents the best fit of a sum of two hyperbolic terms with single values of $IC_{50(1)}$, $IC_{50(2)}$, and F_2 for the three sets of data taken together (i.e., $B_{obsd} = (B_{[A]=0} - B_{[A]\to\infty})\{IC_{50(1)}(1 - F_2)/([A] + IC_{50(1)}) + IC_{50(2)}F_2/([A] + IC_{50(2)})\} + B_{[A]\to\infty}$). The fitted estimates are as follows: log $IC_{50(1)} = -4.54 \pm 0.08$, log $IC_{50(2)} = -2.39 \pm 0.12$, $F_2 = 0.39 \pm 0.03$. There was no significant decrease in the sum of squares with three values of each parameter rather than one ($P > 0.05$). The mean parametric values obtained from fitting the Hill equation to each set of data represented in panels A−D are listed in Table 1.

ing multiple equivalents of receptor and G protein and that the interconversion affects the conformational status of the complex but not the composition.

Preliminary analyses in terms of Scheme 3 indicated that GMP-PNP was without appreciable effect on the affinity of either [^{3}H]quinuclidinylbenzilate or oxotremorine-M for the vacant receptor. A single value of each parameter therefore was assigned to all of the data (i.e., $K_{PR} = K_{PT}$ and $K_{AR} = K_{AT}$). This constraint had no appreciable effect on the goodness of fit or the corresponding sum of squares ($P = 0.08$). Similar agreement emerged for f_{02} and f_{04}, which also could be common to both states (i.e., $f_{R02} = f_{T02}$, $P = 0.07$; $f_{R04} = f_{T04}$, $P > 0.95$). In either state of the receptor, the parameters f_{30}, f_{21}, and f_{12} could be optimized as a single value without increasing the sum of squares ($P = 0.09$). The parameters f_{31}, f_{22}, and f_{13} were highly correlated in both states, and all six parameters could be optimized as a single value ($P = 0.07$). The value of f_{T40} was undefined; it therefore was mapped to identify a range of optimal values and fixed accordingly. A similar examination of K_{RT} indicated that the value was defined only by a lower bound in the absence of nucleotide and only by an upper bound in the presence of GMP-PNP. The value of log K_{RT} therefore was fixed at +3 and −3, respectively. Larger or smaller values were without effect on either the sum of squares or the values of other parameters. The best fit of Scheme 3 to the combined data is illustrated in Figure 11, and the parametric values are listed in Table 5. The weighted sum of squares is 86% of that obtained from the empirical analysis in terms of Scheme 1 (cf. Figure 10).

In terms of the model, the multiple affinities revealed by oxotremorine-M in the absence of nucleotide arise from pronounced negative cooperativity between the second and third equivalents of the agonist (i.e., log $f_{R30} = 2.07$) and a complex blend of negative and positive cooperativity between the agonist and [^{3}H]quinuclidinylbenzilate at different levels of occupancy. The nature of the latter effect has been examined previously (*6*). Owing to the high value of f_{R30}, the third equivalent of oxotremorine binds with a microscopic dissociation constant of 0.1 mM (i.e., log $(f_{R20}f_{R30}K_{AR}) = -3.98$). Since there is comparatively little effect of the first equivalent on the binding of the second (i.e., log $K_{AR} = -6.32$ and log $(f_{R20}K_{AR}) = -6.05$), occupancy of the receptor by oxotremorine-M in the absence of an antagonist is restricted to one-half of the sites at lower concentrations of the agonist (i.e., $< \sim 5\ \mu$M).

GMP-PNP acts to redistribute receptors from the R state to the T state, which results in the introduction of negative cooperativity between the first equivalent of oxotremorine-M and the second (i.e., log $f_{T20} = 2.62$). Occupancy of the

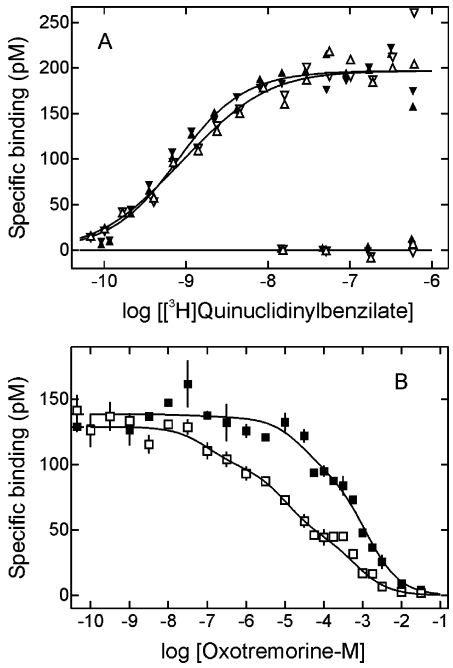

FIGURE 10: Binding of oxotremorine-M and [^{3}H]quinuclidinylbenzilate to M_2 receptor reconstituted with G proteins, analyzed in terms of Scheme 1. (A) Total binding was measured at graded concentrations of [^{3}H]QNB in the absence of guanyl nucleotide (△,▽) and in the presence of 0.1 mM GMP-PNP (▲,▼), either alone (upper curves) or in the presence of 1 mM unlabeled NMS (baseline). The different symbols denote data from two independent experiments (▲,△;▼,▽). (B) Total binding was measured at a half-saturating concentration of [^{3}H]QNB (1.93 ± 0.17 nM, $N = 7$) and graded concentrations of oxo. Most experiments included parallel assays in the absence of guanyl nucleotide (□) and in the presence of 0.1 mM GMP-PNP (■). The lines represent the best fit of Scheme 1 ($n = 3$) to the data represented in panels A and B taken together. The parametric values and further details regarding the analyses are given in Table 4. The mean value of $[R]_t$ used to obtain the adjusted values of B_{obsd} plotted on the *y*-axis is 197 ± 23 pM ($N = 11$). Points shown at the lower end of the *x*-axis in panel B indicate binding in the absence of oxo.

receptor by oxotremorine-M in the absence of an antagonist therefore is restricted to one-quarter of the sites at lower concentrations of the agonist (i.e., log ($f_{T20}K_{AT}$) = −3.70).

DISCUSSION

Assembly of Tetramers from Monomers. Whereas M_2 receptors are extracted from *Sf*9 membranes as oligomers, at least in part (*33*, *41*), they emerge primarily as monomers from affinity chromatography on ABT-Sepharose. Silver staining of gels loaded with the purified M_2 receptor revealed a major band at the position expected for a monomer and a minor band corresponding to a dimer (*42*). Western blots also have shown that the purified receptor migrates wholly or largely as a monomer (*33*). Although oligomers may tend to dissociate under the conditions of electrophoresis, the monomeric status after purification was confirmed by the failure of differently tagged mutants to coprecipitate when purified from coinfected *Sf*9 cells (*28*).

M_2 receptors purified from *Sf*9 cells also were predominantly monomeric in the present investigation. They migrated almost exclusively as monomers during electrophoresis, as revealed by silver staining and immunoblots, and they underwent little or no coprecipitation when the FLAG- and HA-tagged adducts were purified from coinfected cells.

Table 4: Parametric Values for the Binding of Oxotremorine-M to Receptor Reconstituted with G Proteins, Estimated Empirically in Terms of Scheme 1[a]

parameter	no GMP-PNP	0.1 mM GMP-PNP
log K_{A1}	−7.87 ± 0.37	
log K_{A2}	−5.88 ± 0.28	−5.09 ± 0.30
log K_{A3}	−3.46 ± 0.08	
log K_{P1}	−9.56 ± 0.12	−9.16 ± 0.03
log K_{P2}		
log K_{P3}	−8.64 ± 0.08	
F_1	0.18[b]	0.01[b]
F_2	0.31 ± 0.04	
F_3	0.51 ± 0.05	0.68 ± 0.06

[a] The data illustrated in both panels of Figure 10 were pooled and analyzed empirically according to eq 2 ($n = 3$) to obtain the parametric values listed in the table. The parameters K_{Aj} and K_{Pj} denote the affinities of oxo and [^{3}H]QNB, respectively. Those values and the values of F_j were shared where possible between data acquired in the absence and presence of GMP-PNP in order to minimize the number of parameters without appreciably affecting the sum of squares ($P > 0.05$). At least three classes of sites are required to describe the system in terms of the model, but four classes can be observed overall. Single values of K_{A1} and K_{A3} were assigned to all of the data, whereas separate values of K_{A2} were assigned to data acquired in the absence of guanyl nucleotide and in the presence of 0.1 mM GMP-PNP. There was a significant increase in the sum of squares over that from an unconstrained fit if K_{A2} was assumed to be unaffected by GMP-PNP ($P < 0.03$). In the case of [^{3}H]QNB, values of K_{Pj} were assigned separately to data acquired with and without GMP-PNP. Two classes of sites were sufficient in the absence of nucleotide (i.e., $K_{P1} = K_{P2}$), and one class was sufficient in the presence of GMP-PNP (i.e., $K_{P1} = K_{P2} = K_{P3}$). A single value of F_2 was common to all of the data, whereas separate values of F_3 were assigned to data acquired with and without GMP-PNP. Values of $[R]_t$ were assigned separately to data acquired with and without the nucleotide to accommodate small differences in the apparent capacity in some experiments. [b] $F_1 = 1 - F_2 - F_3$.

Immunoreactive bands of higher molecular mass that appeared following cross-linking with BS^3 were comparatively faint, indicating that the monomers were accompanied by only minor populations of dimers and tetramers.

The largely monomeric status is consistent with binding properties that are indicative of identical and mutually independent sites. The capacity was the same for both [^{3}H]-quinuclidinylbenzilate and *N*-[^{3}H]methylscopolamine, and the Hill coefficient in each case was near or indistinguishable from 1; moreover, analyses in terms of Scheme 1 indicated that the two antagonists interact in a competitive manner. The Hill coefficient also was indistinguishable from 1 for the inhibitory effect of the agonist oxotremorine-M on the binding of [^{3}H]quinuclidinylbenzilate.

Reconstitution of the purified monomers into phospholipid vesicles led to the formation of oligomers, most of which appeared to be tetramers. FLAG- and HA-tagged receptors were found to coprecipitate after reconstitution and after the reconstituted material had been resolubilized in digitonin−cholate. Similarly, the effect of BS^3 on electrophoretic mobility was essentially the same regardless of whether the reagent was added to the reconstituted preparation or to the receptor after resolubilization: monomers were virtually eliminated, and the major immunopositive band corresponded in size to a homotetramer. The homomeric nature of the cross-linked complex is supported by the purity of the initial preparation, in which at least 70% of the protein identified by silver staining was M_2 receptor. The survival of reconstituted tetramers upon subsequent dispersal of the phos-

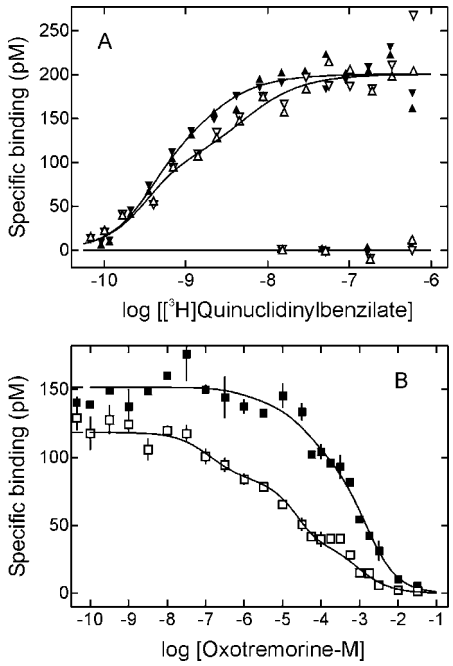

FIGURE 11: Binding of oxotremorine-M and [^{3}H]quinuclidinylbenzilate to M_2 receptor reconstituted with G proteins, analyzed in terms of Scheme 3. The data are the same as those represented in Figure 10, and the lines represent the best fit of Scheme 3 ($n = 4$) to the data in both panels taken together. All parameters were assigned to enforce mechanistic consistency; the fitted values and further details regarding the analyses are given in Table 5. The mean value of $4[R]_t$ used to obtain the adjusted values of B_{obsd} plotted on the *y*-axis is 201 ± 23 pM ($N = 11$). Differences in the relative positions of the fitted curves and corresponding data in Figures 10 and 11 arise from the different constraints imposed by the assignment of parameters in the two models and from the normalization of the data in both panels to a single value of $[R]_t$. Further details are described in the legend to Figure 10.

Table 5: Parametric Values for the Binding of Oxotremorine-M and [^{3}H]Quinuclidinylbenzilate to Receptor Reconstituted with G Proteins, Estimated in Terms of Scheme 3 ($n = 4$)[a]

parameter	R state (no GMP-PNP)	T state (0.1 mM GMP-PNP)
log K_P	−8.64 ± 0.18	
log K_A	−6.32 ± 0.36	
log f_{02}	−1.14 ± 0.43	
log f_{20}	0.27 ± 0.56	2.62 ± 0.42
log f_{11}	−1.33 ± 0.38	2.32 ± 1.17
log f_{03}	1.18 ± 0.44	0.65 ± 0.46
log f_{30}, log f_{21}, log f_{12}	2.07 ± 0.87	−0.90 ± 0.53
log f_{04}	−0.14 ± 0.45	
log f_{40}	−0.34 ± 1.07	2 [b]
log f_{31}, log f_{22}, log f_{13}	−1.36 ± 0.95	
log K_{RT}	+3 [c]	−3 [c]

[a] The data illustrated in both panels of Figure 11 were pooled and analyzed according to eq 4 ($n = 4$) to obtain the parametric values listed in the table. [^{3}H]QNB and oxo were designated as ligands P and A, respectively. All parameters were assigned to enforce mechanistic consistency; therefore, single values of K_{PR}, K_{PT}, f_{R0j}, and f_{T0j} ([^{3}H]QNB), K_{AR}, K_{AT}, f_{Ri0}, and f_{Ti0} (oxo), and f_{Rij} and f_{Tij} ([^{3}H]QNB and oxo) were common to all relevant data acquired with or without GMP-PNP in both panels. Separate values of K_{RT} were assigned to all data acquired in the absence of nucleotide on the one hand and in the presence of GMP-PNP on the other. Some values of *K* and *f* were combined further, as described in the text, in order to minimize the number of parameters without appreciably affecting the sum of squares. [b] The value of log f_{40} in the presence of GMP-PNP (i.e., f_{T40}) was defined only by a lower bound (i.e., log $f_{40} > 2.0$), as determined by mapping. Larger values were without appreciable effect on the sum of squares ($P > 0.05$) or on the values of other parameters. The parameter therefore was fixed as shown in the table. [c] The values of log K_{RT} were fixed during the analysis, as described in the text. The effect is to place the receptors wholly in the R state in the absence of nucleotide (log $K_{RT} = +3$) or wholly in the T state in the presence of GMP-PNP (log $K_{RT} = -3$).

pholipid is consistent with the observation that oligomers of the M_2 receptor can be extracted from *Sf*9 cells, as identified by coimmunoprecipitation (*33*, *41*), and from myocardial membranes, as inferred from noncompetitive effects in the binding of muscarinic ligands (*29*).

Although the reconstituted receptor appeared to be mostly tetrameric, the major band after treatment with BS^3 was accompanied by a weaker and somewhat broader band indicative of larger aggregates. A minor band corresponding to a dimer also was observed in some experiments. Dimers may be formed during the process of reconstitution, perhaps as an intermediate during the assembly of tetramers, or they may derive from tetramers that escape alkylation by BS^3.

Little if any of the coprecipitation found with reconstituted receptors derived from the sequestration of otherwise independent monomers within the same vesicles. Such colocalization can be ruled out by the effect of cross-linking on electrophoretic mobility, which was the same before and after resolubilization. Measurements of resonance energy transfer within oligomers of rhodopsin in liposomes (*43*) and of the NK1 receptor in HEK293 cells (*44*) indicated that the distance between donor and acceptor fluorophores was approximately 50 Å. Similar values have been obtained from molecular modeling of rhodopsin, which suggested that the distance between two monomers within a dimer is 35 Å, and the distance between dimers is 45 Å (*26*). Since the spacer arm of BS^3 is 11 Å long, cross-linking will occur only between receptors that are closely associated within the vesicle. Collisional cross-linking may occur when proteins are reconstituted at a high ratio of protein to lipid (*45*), but it can be prevented at lower ratios. The ratio of phospholipid to M_2 receptor in the current study was over 4,000:1 (w/w), which is 5-fold greater than the ratio that has been shown to prevent the oligomerization of Ca^{2+}-ATPase (*46*) and 10-fold greater than the ratio that prevents the oligomerization of rhodopsin (*47*).

Cross-linked FLAG- and HA-tagged receptors failed to undergo coimmunoprecipitation when incubated with an immobilized anti-FLAG antibody. Moreover, treatment with BS^3 largely precluded immunoprecipitation by an anti-FLAG antibody but had little if any effect on immunoprecipitation by an anti-HA antibody. Cross-linking therefore occurs at least partly at the ϵ-amino group of lysyl residues in the FLAG extension, thereby blocking the interaction with the antibody. There is no lysyl residue within the c-Myc extension, however, and tetramers were the major band detected when BS^3 was added to reconstituted receptors purified from *Sf*9 cells expressing only the c-Myc-tagged receptor. Cross-linked oligomers therefore were not stabilized exclusively via residues in the FLAG sequence.

The formation of tetramers from purified monomers suggests that a vesicular structure is a necessary and sufficient condition for self-assembly. Within the cell, oligomers of G

protein-coupled receptors appear to form prior to their insertion in the plasma membrane. Resonance energy transfer has been detected with various receptors in membranes enriched in endoplasmic reticulum, including the CCR5 receptor (*48*), the oxytocin and vasopressin V1a and V2 receptors (*49*), the α-factor receptor (*50*), and the C5a receptor (*51*). Also, the GB1 and GB2 subunits of the $GABA_B$ receptor both are required for expression of a functional oligomer at the cell surface (*52*, *53*). Similarly, trafficking of the platelet activating factor receptor and the vasopressin V2 receptor from the endoplasmic reticulum to the plasma membrane was shown to be impaired upon co-expression of mutants (*54*, *55*). The assembly of oligomers may be assisted by molecular chaperones (*51*, *56*), although the nature of their involvement remains unclear. An optional role for chaperones is consistent with the observation that oligomers of the C5a receptor form in yeast, which lacks the accessory proteins found in mammalian cells (*51*). In any event, the formation of tetramers from functional monomers in phospholipid vesicles implies that the process of oligomerization is intrinsic to the receptor and not absolutely dependent upon ancillary proteins or the endoplasmic reticulum.

Cooperative Interactions within a Tetramer. Whereas M_2 receptors recovered from ABT-Sepharose behaved as mutually independent monomers, their reconstitution in vesicles led to noncompetitive effects indicative of cooperativity among four interacting sites. The apparent capacity of the reconstituted receptor for *N*-[^{3}H]methylscopolamine was about 50% of that for [^{3}H]quinuclidinylbenzilate, implying that some of the sites were of anomalously weak affinity for *N*-[^{3}H]methylscopolamine; paradoxically, however, the apparent affinity of *N*-methylscopolamine for those sites was significantly higher when inferred from its inhibitory effect on the binding of [^{3}H]quinuclidinylbenzilate. Such a discrepancy is inconsistent with Scheme 1, in which all ligands compete for mutually independent sites. *N*-Methylscopolamine therefore appears to inhibit at sites to which it cannot bind, a noncompetitive effect that cannot be accommodated by Scheme 1 at any value of *n*.

The failure of Scheme 1 rules out any arrangement that can be described in those terms. Formation of an oligomer might introduce a static heterogeneity discerned by *N*-[^{3}H]-methylscopolamine within an otherwise homogeneous population of receptors, but such asymmetry is a special case of Scheme 1 in which each class of sites constitutes the fraction $1/n$ of the total receptor (i.e., $F_j = 1/n$ for all j). Some receptors also might be oriented within the vesicles such that they are accessible to [^{3}H]quinuclidinylbenzilate but not to hydrophilic compounds such as *N*-[^{3}H]methylscopolamine, but that also is a specific case of Scheme 1. Such proposals can account for a difference in the apparent capacity for two radioligands, but they cannot reconcile that difference with the noncompetitive effect of unlabeled *N*-methylscopolamine.

Several considerations suggest that the binding properties are independent of the orientation of receptors within the vesicles, which remains unclear. A subpopulation of inwardly facing sites will lead to a shortfall in capacity only if the vesicles are impermeable to *N*-[^{3}H]methylscopolamine on the time-scale of a binding assay. Since the apparent capacity for *N*-[^{3}H]methylscopolamine was the same after incubation of the reaction mixture for 15 min or 45 min, sequestration can be ruled out by the failure of Scheme 1. Some degree of permeability is implied, however, by the observed effect of GMP-PNP on the binding of oxotremorine-M; G proteins were mixed with the receptor prior to reconstitution and presumably were sequestered within the vesicles as they formed. Moreover, the coimmunoprecipitation of HA- and FLAG-tagged receptors by the anti-FLAG antibody was virtually eliminated by the membrane-impermeable cross-linker BS^3. It therefore appears that the vesicles were permeable to GMP-PNP and presumably to other hydrophilic compounds such as BS^3 and *N*-methylscopolamine.

Effects that appear as discrepancies in terms of Scheme 1 can be accommodated as cooperative interactions in terms of Scheme 2, which provides a satisfactory and mechanistically consistent description of the data taken together. The shortfall in the capacity for *N*-[^{3}H]methylscopolamine can be rationalized as negative homotropic cooperativity that effects a 7-fold reduction in the microscopic dissociation constant of the radioligand after 50% of the sites have been occupied. No comparable effect occurs in the binding of [^{3}H]-quinuclidinylbenzilate, which therefore labels all of the sites at the higher concentrations of radioligand used in the assays. The noncompetitive effect of unlabeled *N*-methylscopolamine arises from heterotropic cooperativity between *N*-methylscopolamine and [^{3}H]quinuclidinylbenzilate.

In the present application of Scheme 2, the system is assumed to be symmetric in the sense that all of the sites on the vacant oligomer are of equal affinity for the ligand. It follows that both the latent sites for *N*-[^{3}H]methylscopolamine and the attendant noncompetitive interaction with [^{3}H]-quinuclidinylbenzilate have been attributed exclusively to cooperativity. That assignment is arbitrary, however, because the possibility that the system is both asymmetric and cooperative cannot be ruled out.

The data are described better by Scheme 2 than by Scheme 1 when n is as low as 2, and the fit of Scheme 2 improves progressively as n is increased to 8. At any value of n greater than 4, however, the AIC_C scores indicate that the additional parameters are redundant. A tetramer therefore emerges as the oligomeric state corresponding to the most efficient form of Scheme 2, in agreement with the electrophoretic mobility of the major band after reconstitution and cross-linking. Although reconstitution might be expected to yield a mixed population of monomers and oligomers, a contingent of monomers is without significant effect on the fit of the model when n exceeds 2; when n is 4, such an analysis indicates that monomers would account for only about 6% of all sites. The absence of any requirement for a subpopulation of mutually independent sites is consistent with the failure to detect monomers on western blots of the receptor after reconstitution and cross-linking. Cross-linked β_2-adrenergic receptors also have been shown to migrate predominantly as multimers (*57*).

In the absence of G protein, reconstituted M_2 receptors bound oxotremorine-M in a featureless manner that points either to monomers or to oligomers that exhibit little or no cooperativity. The latter possibility is favored by the cooperative effects seen in the binding of *N*-methylscopolamine and [^{3}H]quinuclidinylbenzilate under the same conditions and by the electrophoretic mobility of the major band after reconstitution and cross-linking. The inclusion of G

protein led to a GMP-PNP-sensitive dispersion of affinities similar to that observed previously upon purification and subsequent reconstitution of muscarinic and other G protein-coupled receptors (e.g., *34*, *58*−*60*). Scheme 1 affords a good empirical description of such data, including those presented here, but it offers little insight into the underlying molecular events; moreover, it is at variance with the characteristic binding patterns revealed by agonists at G protein-coupled receptors when the model is applied in a mechanistically consistent manner (e.g., refs *8*, *16*, *61*−*63*).

The binding of oxotremorine-M and [^{3}H]quinuclidinylbenzilate to receptor reconstituted with G proteins can be described in a mechanistically explicit and consistent manner by Scheme 3, which was introduced previously to account for the binding of agonists to muscarinic receptors in myocardial membranes (*6*). The fit to the present data is comparable to that obtained from empirical analyses in terms of Scheme 1, which can be taken as a measure of the agreement that would be obtained with the true model if it were known. Cooperativity among four interacting sites therefore can account for the inhibitory effect of oxotremorine-M on the binding of [^{3}H]quinuclidinylbenzilate and for the modulation of that effect by GMP-PNP. The required value of n was confirmed by reducing the number of interacting sites in Scheme 3 from four to two, which resulted in a 1.6-fold increase in the sum of squares and marked deviations between the fitted curves and the data.

In terms of Scheme 3, the multiple affinities revealed by oxotremorine-M arise from negative homotropic cooperativity in the binding of the agonist and from a blend of positive and negative heterotropic cooperativity between the agonist and [^{3}H]quinuclidinylbenzilate. The effect of GMP-PNP is accommodated as a shift in the distribution of vacant receptors from the R state to the T state (i.e., $K_{RT} = [R]/[T]$), which are found to differ only in the degree of homo- and heterotropic cooperativity at various levels of occupancy. GMP-PNP was without discernible effect on the affinity of either oxotremorine-M or quinuclidinylbenzilate for the vacant receptor. The same arrangement has been described previously for the effect of GMP-PNP on the binding of agonists to muscarinic receptors in myocardial membranes (*6*) and to a purified complex of receptor and G protein from porcine atria (*17*). A reciprocal arrangement has been described for the binding of GDP to G proteins labeled by [^{35}S]GTPγS, also in myocardial membranes, where carbachol was found to regulate the distribution of at least two interacting G proteins between two states that differ in their cooperative properties with respect to guanyl nucleotides (*22*).

The foregoing considerations suggest that GMP-PNP acts by regulating the conformational status of a multimeric complex comprising four equivalents of receptor (R) and at least two G proteins (i.e., R_4G_2). Two states are shown in Scheme 3, corresponding to the complex with and without GMP-PNP. If there were two or more equivalents of G protein, the model would require three or more states to accommodate intermediate concentrations of the nucleotide (N) (e.g., $R_4G_2 \rightleftharpoons R_4G_2N \rightleftharpoons R_4G_2N_2$). The allosteric interaction between GMP-PNP and the agonist *in vivo* presumably occurs in the absence of an antagonist, in contrast to the present experiments. Under those conditions, the effect of the nucleotide in terms of Scheme 3 is to reduce binding of the agonist by shifting negative homotropic cooperativity from the second and third equivalents of the agonist (f_{30}, Table 5) to the first and second equivalents (f_{20}).

Scheme 2 and the extended version depicted by Scheme 3 allow the cooperative effects revealed in the binding of antagonists and the multiphasic, nucleotide-sensitive patterns characteristic of agonists to be interpreted within a single mechanistic framework. The assumption of oligomeric homogeneity, which is implicit throughout, is supported by the observation that reconstituted, cross-linked receptors migrated primarily as tetramers. Since G proteins were added at a level sufficient to saturate the receptor, the complement of the resulting heteromer also is likely to be the same throughout the preparation of vesicles and among different preparations. The number of equivalents of G protein within the heteromer is unclear, however, apart from the earlier suggestion that there are at least two.

Restoration of the Native Complex. The binding properties of the reconstituted receptor bear a striking resemblance to those of the muscarinic receptor from mammalian heart. The pattern of latent sites and noncompetitive effects exhibited by *N*-methylscopolamine and quinuclidinylbenzilate is essentially the same as that found previously in two different preparations from porcine atria: a solubilized extract in cholate−NaCl (*29*) and an affinity-purified complex of receptor and G protein (*17*). Similarly, the GMP-PNP-sensitive dispersion of affinities revealed by oxotremorine-M mimics in some detail the pattern described previously for agonists at the muscarinic receptor in myocardial membranes from dog (*10*), rat (*64*), and hamster (*6*, *16*). In common with the receptor in membranes from hamster heart (*6*), at least four classes of sites are required to account empirically for the present data in terms of Scheme 1: three classes are observed in the absence of GMP-PNP (K_{A1}, K_{A2}, K_{A3}); a fourth class arises from a nucleotide-dependent increase in the value of K_{A2}, and the effect is accompanied by a net interconversion of sites from the state of highest affinity (K_{A1}) to that of lowest affinity (K_{A3}). Reconstitution therefore yields a cooperative, tetrameric system that is functionally indistinguishable from the muscarinic receptor in the heart, suggesting that the native arrangement of receptors and G proteins has been recovered *in vitro*.

The shortfall in capacity for *N*-[^{3}H]methylscopolamine is attributed in Scheme 2 to negative homotropic cooperativity between the second and third equivalents of the radioligand (i.e., $\log f_{30} = 0.85$). A similar effect emerges for oxotremorine-M in Scheme 3, where the multiphasic binding profile in the absence of GMP-PNP derives in part from negative homotropic cooperativity between the second and third equivalent of the agonist (i.e., $\log f_{R30} = 2.07$). The apparent capacity for oxotremorine-M therefore is predicted to be about 50% of that for [^{3}H]quinuclidinylbenzilate in assays analogous to those involving *N*-methylscopolamine and [^{3}H]-quinuclidinylbenzilate.

In accord with this expectation, the apparent capacity for [^{3}H]oxotremorine-M was found to be 48% of that for [^{3}H]-quinuclidinylbenzilate in a preparation of membranes from whole rat heart (*65*). Similarly, the capacity for [^{3}H]-oxotremorine-M was 44% of that for *N*-[^{3}H]methylscopolamine in a digitonin-solubilized preparation from rat heart (*66*). Although the capacity for [^{3}H]quinuclidinylbenzilate exceeds that for *N*-[^{3}H]methylscopolamine in some detergents

and after reconstitution, there is no difference with receptor extracted in digitonin (*29*). In studies with [^{3}H]acetylcholine, the apparent capacity of rat atrial membranes for the agonist was 71% of that for the antagonist [^{3}H]4-NMPB (*67*). The apparent capacity for the agonist *cis*-[^{3}H]methyldioxolane was 17% of that for [^{3}H]quinuclidinylbenzilate in homogenates of whole rat heart. Values greater or less than 50% may derive from the expression of negative cooperativity at different levels of occupancy.

Guanyl nucleotides generally have been found to reduce the apparent capacity for radiolabeled agonists with little or no change in their apparent affinity (e.g., refs *67*, *68*), in accord with their effect on the inhibition of radiolabeled antagonists by unlabeled agonists. Similarly, GMP-PNP was without discernible effect on the affinity of oxotremorine-M for the vacant tetramer as inferred from Scheme 3. With the cardiac muscarinic receptor, however, the apparent capacity for a radiolabeled agonist in the presence of the nucleotide generally was below the value that would be consistent with a tetramer (i.e., <25%) (*65*−*68*). Such values imply that the receptor is larger than a tetramer if the nucleotide acts in the manner described here in the context of Scheme 3. Alternatively, the assumption that there are two states differing only in their cooperative properties may be overly restrictive under some conditions.

Size and Composition of the Native Complex. The recovery of native functionality in reconstituted tetramers suggests that the cardiac muscarinic receptor is tetrameric *in vivo*. In other studies, G protein-coupled receptors have appeared in a range of oligomeric sizes, both smaller and larger. Electrophoresis on reducing and nonreducing gels has revealed bands corresponding to both monomers and dimers for several members of the rhodopsin-like family, including the δ-opioid receptor from CHO and COS cells (*69*), the D_3 dopamine receptor from mammalian brain (*70*), the D_2 dopamine receptor from *Sf*9 cells (*71*), the M_3 muscarinic receptor from COS cells (*72*), the β_2-adrenergic receptor from *Sf*9 and HEK293 cells (*57*), the somatostatin receptor from CHO and HEK293 cells (*73*), and rhodopsin from bovine retinal rod outer segment membranes (*74*, *75*). In addition, trimers and tetramers have been reported for the D_2 dopamine receptor (*71*), and tetramers have been reported for the D_3 dopamine receptor (*70*) and the β_2-adrenergic receptor (*57*).

The effects of cross-linking suggest that monomers may form from dimers or that both may form from larger oligomers during solubilization or under the conditions of electrophoresis. Treatment with BS^3 in the present investigation resulted in the disappearance of monomers and the appearance of oligomers, which were mostly tetramers accompanied by some larger aggregates. Similarly, treatment of rod outer segment membranes with DSP led to the appearance of tetramers and larger oligomers of rhodopsin (*75*). The ratio of dimers to monomers was increased by BASED in the case of the β_2-adrenergic receptor (*76*), by DSP in the case of the δ-opioid receptor (*69*), by CuP in the case of the D_2 dopamine receptor (*25*), and by BS^3 in the case of the somatostatin receptor (*73*).

Studies into the oligomeric status of G protein-coupled receptors in whole cells and native membranes have suggested that the basic structural unit may be a dimer in at least some cases. Measurements of fluorescence resonance energy transfer have pointed to dimers of the β-adrenergic receptor (*77*) and the sterile 2 α-factor receptor (*78*). Atomic force microscopy of native mouse disc membranes has revealed that rhodopsin forms extensive paracrystalline arrays that appear to be rows of dimers (*26*, *79*). A dimeric structure for both active and inactive rhodopsin also has been suggested on the basis of hydrodynamic studies (*74*).

Several lines of evidence suggest that the overall complement is an even number of receptors. There is a recurring observation that agonists and antagonists detect a 50:50 mixture of high- and low-affinity sites in preparations of muscarinic and other G protein-coupled receptors (e.g., refs *17*, *29*, *30*, *58*, *80*−*82*). Western blots of the β_2-adrenergic receptor have revealed bands corresponding to dimers, tetramers, and possibly larger multiples thereof (*57*). As noted above, atomic force microscopy of rhodopsin has revealed an array apparently composed of dimers (*26*). Both a trimer and a pentamer are difficult to reconcile with an emerging view that the ratio of receptor to α-subunit within the receptor-G protein complex is 2 to 1 (*26*, *79*, *83*−*85*). Similarly, measurements of surface plasmon resonance have shown that the binding of transducin to rhodopsin saturates at a ratio of 0.6 G protein to 1 receptor (*86*). If oligomers are assembled from dimers, then tetramers of the reconstituted M_2 receptor may form as a dimer of dimers.

The pattern of paired receptors is not universal, however, and electrophoretic bands corresponding to trimers have been identified along with monomers and tetramers of the purified muscarinic receptor (*17*). Bands corresponding to trimers also have been identified on western blots of the D_2 dopamine receptor (*71*) and rhodopsin (*74*, *75*). The AIC_C scores indicate that the fit of Scheme 2 to the present data is optimal with four interacting sites, but comparable agreement is obtained with *n* taken as either three or five.

The reconstituted M_2 receptor shows no evidence of monomers after cross-linking. On the basis of resonance energy transfer, it has been concluded that the β_1- and β_2-adrenergic receptor and the A_{2A} adenosine receptor also exist only as dimers or larger aggregates (*77*, *87*). The prevalence of oligomers in recent studies questions the role and existence of monomers *in vivo*. In early studies, however, biophysical and biochemical evidence supported the notion that rhodopsin exists in monomeric form (reviewed in *45*). More recently, it has been suggested on the basis of fluorescence resonance energy transfer that the NK1 receptor is purely monomeric at physiological concentrations in living cells (*44*). The M_2 muscarinic receptor and possibly the M_1 muscarinic and β_2-adrenergic receptors can be purified as ligand-binding monomers from *Sf*9 cells (*28*, *42*); similarly, the M_2 receptor purified from heart has been found to behave as a monomer in hydrodynamic studies (*88*). The recovery of tetramers upon reconstitution of the M_2 receptor suggests, however, that the monomeric form may be an artifact of purification. If the Gα-subunit associates with a dimeric receptor (*26*, *79*, *83*−*85*), the physiological role of monomers, if it exists, may not involve a direct interaction with G proteins.

Although monomers bind antagonists with characteristic affinity, at least in the case of the M_2 receptor (*28*), various studies have suggested that oligomers are required for a response (e.g., refs *20*, *89*−*91*). Coexpression of wild-type and mutant α-factor receptors led to proper binding of ligands but no response (*56*), and similar results have been reported for the 5-HT_{2C} receptor (*85*). It is not always clear, however,

whether the lack of a response derives from a malfunctioning oligomer or from its failure to appear on the plasma membrane. Oligomers also may be required for the proper interaction with the G protein. Finally, the functional unit that elicits a response may correspond to the basic structural unit, or it may be larger. The degree of amplification that has been reported for the activation of transducin by rhodopsin (*92*) and for the activation of a chemoreceptor-regulated kinase (*93*) suggests that cooperative interactions may propagate through an array that is considerably larger than a dimer or a tetramer. The existence of such aggregates may account for the slowest moving bands observed with cross-linked M_2 receptors on western blots.

The cooperative models examined here provide a mechanistically consistent description of effects in a reconstituted system that closely resembles the M_2 muscarinic receptor in myocardial preparations. Their success, taken with the limitations of alternative schemes, is consistent with the notion that cooperativity in the binding of agonists on the one hand and guanyl nucleotides on the other is a determinant of signaling at the level of the receptor and the G protein (*6*, *17*). It follows that oligomers of G protein-coupled receptors may exist to host such effects, thereby creating the mechanistic pathway for transduction. An explicit mechanistic model is likely to prove useful in further work on G protein-mediated signaling and its dysfunction in disease.

REFERENCES

1. Gilman, A. G. (1987) G proteins: transducers of receptor-generated signals, *Annu. Rev. Biochem. 56*, 615−649.
2. Birnbaumer, L., Abramowitz, J., and Brown, A. M. (1990) Receptor-effector coupling by G proteins, *Biochim. Biophys. Acta 1031*, 163−224.
3. Milligan, G. (2001) Oligomerisation of G protein-coupled receptors, *J. Cell Sci. 114*, 1265−1271.
4. Angers, S., Salahpour, A., and Bouvier, M. (2002) Dimerization: an emerging concept for G protein-coupled receptor ontogeny and function, *Annu. Rev. Pharmacol. Toxicol. 42*, 409−435.
5. Park, P. S., Filipek, S., Wells, J. W., and Palczewski, K. (2004) Oligomerization of G protein-coupled receptors: past, present, and future, *Biochemistry 43*, 15643−15656.
6. Chidiac, P., Green, M. A., Pawagi, A. B., and Wells, J. W. (1997) Cardiac muscarinic receptors. Cooperativity as the basis for multiple states of affinity, *Biochemistry 36*, 7361−7379.
7. Birdsall, N. J., Burgen, A. S., and Hulme, E. C. (1977) Correlation between the binding properties and pharmacological responses of muscarinic receptors, *Adv. Behav. Biol. 24*, 25−33.
8. Kent, R. S., De Lean, A., and Lefkowitz, R. J. (1980) A quantitative analysis of β-adrenergic receptor interactions: resolution of high and low affinity states of the receptor by computer modeling of ligand binding data, *Mol. Pharmacol. 17*, 14−23.
9. Ehlert, F. J. (1985) The relationship between muscarinic receptor occupancy and adenylate cyclase inhibition in the rabbit myocardium, *Mol. Pharmacol. 28*, 410−421.
10. Mattera, R., Pitts, B. J., Entman, M. L., and Birnbaumer, L. (1985) Guanine nucleotide regulation of a mammalian myocardial muscarinic receptor system. Evidence for homo- and heterotropic cooperativity in ligand binding analyzed by computer-assisted curve fitting, *J. Biol. Chem. 260*, 7410−7421.
11. Levitzki, A. (1986) β-adrenergic receptors and their mode of coupling to adenylate cyclase, *Physiol. Rev. 66*, 819−854.
12. De Lean, A., Stadel, J. M., and Lefkowitz, R. J. (1980) A ternary complex model explains the agonist-specific binding properties of the adenylate cyclase-coupled β-adrenergic receptor, *J. Biol. Chem. 255*, 7108−7117.
13. Green, M. A., Chidiac, P., and Wells, J. W. (1997) Cardiac muscarinic receptors. Relationship between the G protein and multiple states of affinity, *Biochemistry 36*, 7380−7394.
14. Neubig, R. R., Gantzos, R. D., and Brasier, R. S. (1985) Agonist and antagonist binding to α_2-adrenergic receptors in purified membranes from human platelets. Implications of receptor-inhibitory nucleotide-binding protein stoichiometry, *Mol. Pharmacol. 28*, 475−486.
15. Lee, T. W., Sole, M. J., and Wells, J. W. (1986) Assessment of a ternary model for the binding of agonists to neurohumoral receptors, *Biochemistry 25*, 7009−7020.
16. Wong, H. M., Sole, M. J., and Wells, J. W. (1986) Assessment of mechanistic proposals for the binding of agonists to cardiac muscarinic receptors, *Biochemistry 25*, 6995−7008.
17. Wreggett, K. A., and Wells, J. W. (1995) Cooperativity manifest in the binding properties of purified cardiac muscarinic receptors, *J. Biol. Chem. 270*, 22488−22499.
18. Rebois, R. V., Warner, D. R., and Basi, N. S. (1997) Does subunit dissociation necessarily accompany the activation of all heterotrimeric G proteins? *Cell. Signalling 9*, 141−151.
19. Chidiac, P. (1998) Rethinking receptor-G protein-effector interactions, *Biochem. Pharmacol. 55*, 549−556.
20. Lachance, M., Ethier, N., Wolbring, G., Schnetkamp, P. P., and Hebert, T. E. (1999) Stable association of G proteins with β_2AR is independent of the state of receptor activation, *Cell. Signalling 11*, 523−533.
21. Gales, C., VanDurm, J. J., Schaak, S., Pontier, S., Percherancier, Y., Audet, M., Paris, H., and Bouvier, M. (2006) Probing the activation-promoted structural rearrangements in preassembled receptor-G protein complexes, *Nat. Struct. Mol. Biol. 13*, 778−786.
22. Chidiac, P., and Wells, J. W. (1992) Effects of adenyl nucleotides and carbachol on cooperative interactions among G proteins, *Biochemistry 31*, 10908−10921.
23. Maggio, R., Vogel, Z., and Wess, J. (1993) Coexpression studies with mutant muscarinic/adrenergic receptors provide evidence for intermolecular "cross-talk" between G protein-linked receptors, *Proc. Natl. Acad. Sci. U.S.A. 90*, 3103−3107.
24. Gouldson, P. R., Higgs, C., Smith, R. E., Dean, M. K., Gkoutos, G. V., and Reynolds, C. A. (2000) Dimerization and domain swapping in G protein-coupled receptors: a computational study, *Neuropsychopharmacology 23*, S60−S77.
25. Guo, W., Shi, L., and Javitch, J. A. (2003) The fourth transmembrane segment forms the interface of the dopamine D_2 receptor homodimer, *J. Biol. Chem. 278*, 4385−4388.
26. Fotiadis, D., Liang, Y., Filipek, S., Saperstein, D. A., Engel, A., and Palczewski, K. (2004) The G protein-coupled receptor rhodopsin in the native membrane, *FEBS Lett. 564*, 281−288.
27. Fotiadis, D., Jastrzebska, B., Philippsen, A., Muller, D. J., Palczewski, K., and Engel, A. (2006) Structure of the rhodopsin dimer: a working model for G protein-coupled receptors, *Curr. Opin. Struct. Biol. 16*, 252−259.
28. Park, P. S., and Wells, J. W. (2003) Monomers and oligomers of the M_2 muscarinic cholinergic receptor purified from *Sf*9 cells, *Biochemistry 42*, 12960−12971.
29. Park, P. S., Sum, C. S., Pawagi, A. B., and Wells, J. W. (2002) Cooperativity and oligomeric status of cardiac muscarinic cholinergic receptors, *Biochemistry 41*, 5588−5604.
30. Armstrong, D., and Strange, P. G. (2001) Dopamine D_2 receptor dimer formation: evidence from ligand binding, *J. Biol. Chem. 276*, 22621−22629.
31. Vivo, M., Lin, H., and Strange, P. G. (2006) Investigation of cooperativity in the binding of ligands to the D_2 dopamine receptor, *Mol. Pharmacol. 69*, 226−235.
32. Javitch, J. A. (2004) The ants go marching two by two: oligomeric structure of G protein-coupled receptors, *Mol. Pharmacol. 66*, 1077−1082.
33. Park, P., Sum, C. S., Hampson, D. R., Van Tol, H. H. M., and Wells, J. W. (2001) Nature of the oligomers formed by muscarinic M_2 acetylcholine receptors in *Sf*9 cells, *Eur. J. Pharmacol. 421*, 11−22.
34. Haga, K., Haga, T., and Ichiyama, A. (1986) Reconstitution of the muscarinic acetylcholine receptor. Guanine nucleotide-sensitive high affinity binding of agonists to purified muscarinic receptors reconstituted with GTP-binding proteins (G_i and G_o), *J. Biol. Chem. 261*, 10133−10140.
35. Rasband, W. S. *ImageJ*, U.S. National Institutes of Health, Bethesda, MD, USA, http://rsb.info.nih.gov/ij, 1997−2006.
36. Wells, J. W. (1992) In *Receptor-Ligand Interactions. A Practical Approach* (Hulme, E. C., Ed.) pp 289−395, Oxford University Press, Oxford, England.

37. Motulsky, H. J., and Christopoulos, A. (2003) *Fitting Models to Biological Data Using Linear and Nonlinear Regression. A Practical Guide to Curve Fitting.* Graphpad Softward Inc., San Diego, CA.
38. Stiles, G. L., Benovic, J. L., Caron, M. G., and Lefkowitz, R. J. (1984) Mammalian β-adrenergic receptors. Distinct glycoprotein populations containing high mannose or complex type carbohydrate chains, *J. Biol. Chem. 259*, 8655−8663.
39. Sum, C. S., Pyo, N., and Wells, J. W. (2001) Apparent capacity of cardiac muscarinic receptors for different radiolabeled antagonists, *Biochem. Pharmacol. 62*, 829−851.
40. Sum, C. S., Park, P. S., and Wells, J. W. (2002) Effects of *N*-ethylmaleimide on conformational equilibria in purified cardiac muscarinic receptors, *J. Biol. Chem. 277*, 36188−36203.
41. Park, P. S., and Wells, J. W. (2004) Oligomeric potential of the M_2 muscarinic cholinergic receptor, *J. Neurochem. 90*, 537−548.
42. Parker, E. M., Kameyama, K., Higashijima, T., and Ross, E. M. (1991) Reconstitutively active G protein-coupled receptors purified from baculovirus-infected insect cells, *J. Biol. Chem. 266*, 519−527.
43. Mansoor, S. E., Palczewski, K., and Farrens, D. L. (2006) Rhodopsin self-associates in asolectin liposomes, *Proc. Natl. Acad. Sci. U.S.A. 103*, 3060−3065.
44. Meyer, B. H., Segura, J. M., Martinez, K. L., Hovius, R., George, N., Johnsson, K., and Vogel, H. (2006) FRET imaging reveals that functional neurokinin-1 receptors are monomeric and reside in membrane microdomains of live cells, *Proc. Natl. Acad. Sci. U.S.A. 103*, 2138−2143.
45. Chabre, M., and le Maire, M. (2005) Monomeric G protein-coupled receptor as a functional unit, *Biochemistry 44*, 9395−9403.
46. Heegaard, C. W., le Maire, M., Gulik-Krzywicki, T., and Moller, J. V. (1990) Monomeric state and Ca^{2+} transport by sarcoplasmic reticulum Ca^{2+}-ATPase, reconstituted with an excess of phospholipid, *J. Biol. Chem. 265*, 12020−12028.
47. Botelho, A. V., Huber, T., Sakmar, T. P., and Brown, M. F. (2006) Curvature and hydrophobic forces drive oligomerization and modulate activity of rhodopsin in membranes, *Biophys. J. 91*, 4464−4477.
48. Issafras, H., Angers, S., Bulenger, S., Blanpain, C., Parmentier, M., Labbe-Jullie, C., Bouvier, M., and Marullo, S. (2002) Constitutive agonist-independent CCR5 oligomerization and antibody-mediated clustering occurring at physiological levels of receptors, *J. Biol. Chem. 277*, 34666−34673.
49. Terrillon, S., Durroux, T., Mouillac, B., Breit, A., Ayoub, M. A., Taulan, M., Jockers, R., Barberis, C., and Bouvier, M. (2003) Oxytocin and vasopressin V1a and V2 receptors form constitutive homo- and heterodimers during biosynthesis, *Mol. Endocrinol. 17*, 677−691.
50. Overton, M. C., Chinault, S. L., and Blumer, K. J. (2003) Oligomerization, biogenesis, and signaling is promoted by a glycophorin A-like dimerization motif in transmembrane domain 1 of a yeast G protein-coupled receptor, *J. Biol. Chem. 278*, 49369−49377.
51. Floyd, D. H., Geva, A., Bruinsma, S. P., Overton, M. C., Blumer, K. J., and Baranski, T. J. (2003) C5a receptor oligomerization. II. Fluorescence resonance energy transfer studies of a human G protein-coupled receptor expressed in yeast, *J. Biol. Chem. 278*, 35354−35361.
52. White, J. H., Wise, A., Main, M. J., Green, A., Fraser, N. J., Disney, G. H., Barnes, A. A., Emson, P., Foord, S. M., and Marshall, F. H. (1998) Heterodimerization is required for the formation of a functional $GABA_B$ receptor, *Nature 396*, 679−682.
53. Galvez, T., Duthey, B., Kniazeff, J., Blahos, J., Rovelli, G., Bettler, B., Prezeau, L., and Pin, J. P. (2001) Allosteric interactions between GB1 and GB2 subunits are required for optimal $GABA_B$ receptor function, *EMBO J. 20*, 2152−2159.
54. Zhu, X., and Wess, J. (1998) Truncated V2 vasopressin receptors as negative regulators of wild-type V2 receptor function, *Biochemistry 37*, 15773−15784.
55. Le Gouill, C., Parent, J. L., Caron, C. A., Gaudreau, R., Volkov, L., Rola-Pleszczynski, M., and Stankova, J. (1999) Selective modulation of wild-type receptor functions by mutants of G protein-coupled receptors, *J. Biol. Chem. 274*, 12548−12554.
56. Overton, M. C., and Blumer, K. J. (2000) G protein-coupled receptors function as oligomers *in vivo*, *Curr. Biol. 10*, 341−344.
57. Salahpour, A., Bonin, H., Bhalla, S., Petaja-Repo, U., and Bouvier, M. (2003) Biochemical characterization of β_2-adrenergic receptor dimers and oligomers, *Biol. Chem. 384*, 117−123.
58. Tota, M. R., Kahler, K. R., and Schimerlik, M. I. (1987) Reconstitution of the purified porcine atrial muscarinic acetylcholine receptor with purified porcine atrial inhibitory guanine nucleotide binding protein, *Biochemistry 26*, 8175−8182.
59. Florio, V. A., and Sternweis, P. C. (1989) Mechanisms of muscarinic receptor action on G_o in reconstituted phospholipid vesicles, *J. Biol. Chem. 264*, 3909−3915.
60. Ikegaya, T., Nishiyama, T., Haga, K., Haga, T., Ichiyama, A., Kobayashi, A., and Yamazaki, N. (1990) Interaction of atrial muscarinic receptors with three kinds of GTP-binding proteins, *J. Mol. Cell. Cardiol. 22*, 343−351.
61. Steinberg, G. H., Eppel, J. G., Kandel, M., Kandel, S. I., and Wells, J. W. (1985) H_2 histaminic receptors in rat cerebral cortex. 1. Binding of [^{3}H]histamine, *Biochemistry 24*, 6095−6107.
62. Steinberg, G. H., Kandel, M., Kandel, S. I., and Wells, J. W. (1985) H_2 histaminic receptors in rat cerebral cortex. 3. Inhibition of [^{3}H]-histamine by H_2 agonists, *Biochemistry 24*, 6115−6125.
63. Sinkins, W. G., and Wells, J. W. (1993) G protein-linked receptors labeled by [^{3}H]histamine in guinea pig cerebral cortex. II. Mechanistic basis for multiple states of affinity, *Mol. Pharmacol. 43*, 583−594.
64. Burgen, A. S. (1987) The effects of agonists on the components of the cardiac muscarinic receptor, *Br. J. Pharmacol. 92*, 327−332.
65. Waelbroeck, M., Robberecht, P., Chatelain, P., and Christophe, J. (1982) Rat cardiac muscarinic receptors. I. Effects of guanine nucleotides on high- and low-affinity binding sites, *Mol. Pharmacol. 21*, 581−588.
66. Berrie, C. P., Birdsall, N. J., Hulme, E. C., Keen, M., and Stockton, J. M. (1984) Solubilization and characterization of guanine nucleotide-sensitive muscarinic agonist binding sites from rat myocardium, *Br. J. Pharmacol. 82*, 853−861.
67. Gurwitz, D., Kloog, Y., and Sokolovsky, M. (1985) High affinity binding of [^{3}H]acetylcholine to muscarinic receptors. Regional distribution and modulation by guanine nucleotides, *Mol. Pharmacol. 28*, 297−305.
68. Gillard, M., Waelbroeck, M., and Christophe, J. (1987) Muscarinic receptor heterogeneity in rat central nervous system. II. Brain receptors labeled by [^{3}H]oxotremorine-M correspond to heterogeneous M_2 receptors with very high affinity for agonists, *Mol. Pharmacol. 32*, 100−108.
69. Cvejic, S., and Devi, L. A. (1997) Dimerization of the δ-opioid receptor: implication for a role in receptor internalization, *J. Biol. Chem. 272*, 26959−26964.
70. Nimchinsky, E. A., Hof, P. R., Janssen, W. G., Morrison, J. H., and Schmauss, C. (1997) Expression of dopamine D_3 receptor dimers and tetramers in brain and in transfected cells, *J. Biol. Chem. 272*, 29229−29237.
71. Zawarynski, P., Tallerico, T., Seeman, P., Lee, S. P., O'Dowd, B. F., and George, S. R. (1998) Dopamine D_2 receptor dimers in human and rat brain, *FEBS Lett. 441*, 383−386.
72. Zeng, F. Y., and Wess, J. (1999) Identification and molecular characterization of M_3 muscarinic receptor dimers, *J. Biol. Chem. 274*, 19487−19497.
73. Grant, M., Collier, B., and Kumar, U. (2004) Agonist-dependent dissociation of human somatostatin receptor 2 dimers: a role in receptor trafficking, *J. Biol. Chem. 279*, 36179−36183.
74. Medina, R., Perdomo, D., and Bubis, J. (2004) The hydrodynamic properties of dark- and light-activated states of *n*-dodecyl β-D-maltoside-solubilized bovine rhodopsin support the dimeric structure of both conformations, *J. Biol. Chem. 279*, 39565−39573.
75. Jastrzebska, B., Maeda, T., Zhu, L., Fotiadis, D., Filipek, S., Engel, A., Stenkamp, R. E., and Palczewski, K. (2004) Functional characterization of rhodopsin monomers and dimers in detergents, *J. Biol. Chem. 279*, 54663−54675.
76. Hebert, T. E., Moffett, S., Morello, J. P., Loisel, T. P., Bichet, D. G., Barret, C., and Bouvier, M. (1996) A peptide derived from a β_2-adrenergic receptor transmembrane domain inhibits both receptor dimerization and activation, *J. Biol. Chem. 271*, 16384−16392.
77. Mercier, J. F., Salahpour, A., Angers, S., Breit, A., and Bouvier, M. (2002) Quantitative assessment of β_1- and β_2-adrenergic receptor homo- and heterodimerization by bioluminescence resonance energy transfer, *J. Biol. Chem. 277*, 44925−44931.

78. Raicu, V., Jansma, D. B., Miller, R. J., and Friesen, J. D. (2005) Protein interaction quantified *in vivo* by spectrally resolved fluorescence resonance energy transfer, *Biochem. J. 385*, 265−277.
79. Liang, Y., Fotiadis, D., Filipek, S., Saperstein, D. A., Palczewski, K., and Engel, A. (2003) Organization of the G protein-coupled receptors rhodopsin and opsin in native membranes, *J. Biol. Chem. 278*, 21655−21662.
80. Peterson, G. L., Herron, G. S., Yamaki, M., Fullerton, D. S., and Schimerlik, M. I. (1984) Purification of the muscarinic acetylcholine receptor from porcine atria, *Proc. Natl. Acad. Sci. U.S.A. 81*, 4993−4997.
81. Potter, L. T., Ferrendelli, C. A., and Hanchett, H. E. (1988) Two affinity states of M_1 muscarine receptors, *Cell. Mol. Neurobiol. 8*, 181−191.
82. Munshi, R., and Linden, J. (1990) Interaction of purified bovine brain A_1-adenosine receptors with guanine nucleotide-binding proteins of human platelet membranes following reconstitution, *Mol. Pharmacol. 38*, 170−176.
83. Baneres, J. L., and Parello, J. (2003) Structure-based analysis of GPCR function: evidence for a novel pentameric assembly between the dimeric leukotriene B_4 receptor BLT1 and the G protein, *J. Mol. Biol. 329*, 815−829.
84. Filipek, S., Krzysko, K. A., Fotiadis, D., Liang, Y., Saperstein, D. A., Engel, A., and Palczewski, K. (2004) A concept for G protein activation by G protein-coupled receptor dimers: the transducin/rhodopsin interface, *Photochem. Photobiol. Sci. 3*, 628−638.
85. Herrick-Davis, K., Grinde, E., Harrigan, T. J., and Mazurkiewicz, J. E. (2005) Inhibition of serotonin 5-hydroxytryptamine$_{2C}$ receptor function through heterodimerization: receptor dimers bind two molecules of ligand and one G protein, *J. Biol. Chem. 280*, 40144−40151.
86. Alves, I. D., Park, C. K., and Hruby, V. J. (2005) Plasmon resonance methods in GPCR signaling and other membrane events, *Curr. Protein Pept. Sci. 6*, 293−312.
87. Canals, M., Burgueno, J., Marcellino, D., Cabello, N., Canela, E. I., Mallol, J., Agnati, L., Ferre, S., Bouvier, M., Fuxe, K., Ciruela, F., Lluis, C., and Franco, R. (2004) Homodimerization of adenosine A_{2A} receptors: qualitative and quantitative assessment by fluorescence and bioluminescence energy transfer, *J. Neurochem. 88*, 726−734.
88. Peterson, G. L., Rosenbaum, L. C., Broderick, D. J., and Schimerlik, M. I. (1986) Physical properties of the purified cardiac muscarinic acetylcholine receptor, *Biochemistry 25*, 3189−3202.
89. Neubig, R. R., Gantzos, R. D., and Thomsen, W. J. (1988) Mechanism of agonist and antagonist binding to α_2 adrenergic receptors: evidence for a precoupled receptor-guanine nucleotide protein complex, *Biochemistry 27*, 2374−2384.
90. Munshi, R., Pang, I. H., Sternweis, P. C., and Linden, J. (1991) A_1 adenosine receptors of bovine brain couple to guanine nucleotide-binding proteins G_{i1}, G_{i2}, and G_o, *J. Biol. Chem. 266*, 22285−22289.
91. Gales, C., Rebois, R. V., Hogue, M., Trieu, P., Breit, A., Hebert, T. E., and Bouvier, M. (2005) Real-time monitoring of receptor and G protein interactions in living cells, *Nat. Methods 2*, 177−184.
92. Kwok-Keung, F. B., and Stryer, L. (1980) Photolyzed rhodopsin catalyzes the exchange of GTP for bound GDP in retinal rod outer segments, *Proc. Natl. Acad. Sci. U.S.A. 77*, 2500−2504.
93. Sourjik, V., and Berg, H. C. (2004) Functional interactions between receptors in bacterial chemotaxis, *Nature 428*, 437−441.

BI6026105